THE UNIVERSITY OF ALBERTA

# FINITE ELEMENT MESH GENERATION

# FOR SEMICONDUCTOR DEVICE SIMULATION

BY

Kris Yau-Kuen Chau

A THESIS

SUBMITTED TO THE FACULTY OF GRADUATE STUDIES AND RESEARCH IN PARTIAL FULFILMENT OF THE REQUIREMENTS FOR THE DEGREE OF MASTER OF SCIENCE.

DEPARTMENT OF ELECTRICAL ENGINEERING

EDMONTON, ALBERTA

SPRING 1988

Permission has been granted to the National Library of Canada to microfilm this thesis and to lend or sell copies of the film.

The author (copyright owner) has reserved other publication rights, and neither the thesis nor extensive extracts from it may be printed or otherwise reproduced without his/her written permission.

L'autorisation a été accordée à la Bibliothèque nationale du Canada de microfilmer cette thèse et de prêter ou de vendre des exemplaires du film.

L'auteur (titulaire du droit d'auteur) se réserve les autres droits de publication; ni la thèse ni de longs extraits de celle-ci ne doivent être imprimés ou autrement reproduits sans son autorisation écrite.

ISBN 0-315-42821-X

THE UNIVERSITY OF ALBERTA

RELEASE FORM

NAME OF AUTHOR: Kris Yau-Kuen Chau

TITLE OF THESIS: Finite Element Mesh Generation for Semiconductor Device Simulation

DEGREE: Master of Science

YEAR THIS DEGREE GRANTED: 1988

Permission is hereby granted to THE UNIVERSITY OF ALBERTA LIBRARY to reproduce single copies of this thesis and to lend or sell such copies for private, scholarly or scientific research purposes only.

The author reserves other publication rights, and neither the thesis nor extensive extracts from it may be printed or otherwise reproduced without the author's written permission.

K Chau

Student's signature

10/F, 173A,
Yee Kuk Street,
Sham Shui Po, Kowloon,
Hong Kong.

Date: April 25, 1988

THE UNIVERSITY OF ALBERTA

FACULTY OF GRADUATE STUDIES AND RESEARCH

The undersigned certify that they have read, and recommend to the Faculty of Graduate Studies and Research for acceptance, a thesis entitled Finite Element Mesh Generation for Semiconductor Device Simulation, submitted by Kris Yau-Kuen Chau, in partial fulfilment of the requirements for the degree of Master of Science.

.....

.....

Supervisors

.....

.....

.....

Date: April 25, 1988

献给

我的爸妈家人

和我深爱的雪琼

## ABSTRACT

In this thesis, we present a new triangular mesh generation mechanism for plane geometry to provide data for a magnetic field sensor simulation program. This scheme is based on a hybrid and modular approach which combines two types of triangulations : Delaunay and regular triangulation. The mechanism also provides experienced users with mesh modification capabilities to edit the initial mesh.

This work aims at extending the capability of the existing mesh generator in 'ALBERTINA', a semiconductor device simulation package for simulating magnetic field sensors. A prototype mesh generator based on the proposed mechanism is implemented in C language with the support of the SunView graphic interface.

The hybrid mesh generator is incorporated into ALBERTINA. The practical applications of the mesh generator are illustrated by considering simulation work analogous to that commissioned recently by an important sensor manufacturing company. This involves the simulation of Hall plate devices.

## ACKNOWLEDGEMENTS

The author would like to thank his supervisors, Professors Dr. H. P. Baltes and W. B. Joerg, for their guidance, encouragement, financial support and many helpful discussions.

Special thanks to Professor Dr. W. Allegretto for helpful advice, encouragement and stimulating discussions.

The author also wishes to thank fellow students D. Briglio, A. Nathan and R. Saad for their invaluable assistance, suggestion and inspiration.

The author gratefully acknowledges the support from the Alberta Microelectronic Center for providing the necessary computing resources.

## TABLE OF CONTENTS


| Chapter | | Page |
|---|---|---|
| 1. | INTRODUCTION | 1 |
| 2. | CONCEPT OF HYBRID APPROACH | 12 |
| | 2.1 Objectives of Finite Element Mesh Generation | 12 |
| | 2.2 Hybrid Mesh Generation Approach | 14 |
| | 2.3 Albertina Framework : Overall Hierarchy | 17 |
| | 2.4 Data Structures for the Hybrid Mesh Generator | 18 |
| 3. | HYBRID MESH GENERATION | 30 |
| | 3.1 Decomposition of Device Region | 30 |
| | 3.2 Hybrid (Delaunay and Regular) Triangulation | 33 |
| | 3.3 Mesh Modification | 34 |
| | 3.4 Achievement and Limitations | 36 |
| 4. | FINITE ELEMENT METHOD AND ANALYSIS OF HALL PLATES | 51 |
| | 4.1 Scheme of Finite Element Method | 51 |
| | 4.2 Analysis of Hall Plate Devices | 52 |
| 5. | RESULTS: A CASE OF COMMERCIAL APPLICATION | 59 |
| | 5.1 Simulation strategy for Hall Plate Devices | 59 |
| | 5.2 Simulation Results for Hall Plate Devices | 61 |
| | 5.3 Mesh and Simulation results for Lateral Magnetotransistor | 62 |
| 6. | CONCLUSION AND OUTLOOK | 75 |
| 7. | REFERENCES | 77 |
| APPENDIX (MESH EXAMPLES) | | 82 |

## LIST OF TABLES


| Table | | Page |
|---|---|---|
| Table 5.1 | Hall Voltage Measurement for Hall Plate Devices(C=D) | 51 |
| Table 5.2 | Hall Voltage Measurement for Hall Plate Devices(C≠D) | 70 |

## LIST OF FIGURES


| Figure | | Page |
|---|---|---|
| Fig. 1.1 | Main modules of mesh generator | 9 |
| Fig. 1.2 | Refinement of the mesh generation problem | 10 |
| Fig. 1.3 | Screen layout for mesh generator | 11 |
| Fig. 2.1 | Regular triangulation steps | 21 |
| Fig. 2.2 | Typical regular triangulation for rectangular region | 22 |
| Fig. 2.3 | Triangulate the inner region | 23 |
| Fig. 2.4 | Triangulate along the boundary strip | 24 |
| Fig. 2.5 | Typical Delaunay triangulation for rectangular region | 25 |
| Fig. 2.6 | User's perception of ALBERTINA | 26 |
| Fig. 2.7 | Conceptual data structure of device domains | 27 |

| | | |
|---|---|---|
| Fig. 2.8 | Data representation for device domains | 28 |
| Fig. 2.9 | Data representation for triangular mesh | 29 |
| Fig. 3.1 | Example of device domains with reflex vertices | 38 |
| Fig. 3.2 | Visible boundary from vertex VR1 | 39 |
| Fig. 3.3 | Visible vertices from VR1 | 39 |
| Fig. 3.4 | Cases in which separator S fails to resolve reflex vertex VR1 | 40 |
| Fig. 3.5 | Possible candidates of separator end points (inside inner cone) | 41 |
| Fig. 3.6 | Use separator S to resolve VR will introduce narrowing at N | 41 |
| Fig. 3.7 | Resulting interior angle of inserting a separator | 42 |
| Fig. 3.8 | Resulting device regions after decomposition | 42 |
| Fig. 3.9 | Device geometry with five subdomains | 43 |

| | | |
|---|---|---|
| Fig. 3.10 | Regular triangulation inside rectangular subdomain | 44 |
| Fig. 3.11 | Hybrid mesh of device with five subdomains | 45 |
| Fig. 3.12 | Initial mesh with 594 elements | 46 |
| Fig. 3.13 | Edited mesh with 448 elements | 47 |
| Fig. 3.14 | Edited mesh with 748 elements | 47 |
| Fig. 3.15 | Mesh with inhomogeneous mesh density | 48 |
| Fig. 3.16 | Mirroring functions of mesh modification | 49 |
| Fig. 3.17 | Abrupt change in triangulation parameter | 50 |
| Fig. 4.1 | Hall voltage in rectangular semiconductor sample | 57 |
| Fig. 4.2 | Hall plate device in the shape of an octagon | 57 |
| Fig. 4.3 | Top view of Hall plate device with contacts | 58 |
| Fig. 5.1 | Device domain of Hall plate device | 63 |
| Fig. 5.2 | Four types of device geometry setup | 64 |

| | | |
|---|---|---|
| Fig. 5.3 | Steps involved in generating symmetric mesh | 65 |
| Fig. 5.4 | Plot of Hall voltage vs effective L/W | 67 |
| Fig. 5.5 | Plot of equipotential lines for Hall plate device | 68 |
| Fig. 5.6 | Plot of current density flow for Hall plate device | 69 |
| Fig. 5.7 | Two dimensional geometry of base region in magnetotransistor | 72 |
| Fig. 5.8 | Mesh of emitter-base region in magnetotransistor | 73 |
| Fig. 5.9 | Equipotential lines at emitter vicinity for $V_{BE}$=0.85V and B=2T | 74 |
| Fig. 5.10 | Minority (electron) carrier density flow lines at emitter | 74 |

## LIST OF SYMBOLS

| Symbol | Name | Unit |
|---|---|---|
| $\mathbf{B}$ | Magnetic induction vector | tesla |
| $D_n$ | Electron diffusion constant | $cm^2/sec$ |
| $D_p$ | Hole diffusion constant | $cm^2/sec$ |
| E | Electric field | volt/cm |
| J | Current density | $ampere/cm^2$ |
| $J_n$ | Electron current density | $ampere/cm^2$ |
| n | Electron concentration | $cm^{-3}$ |
| p | Hole concentration | $cm^{-3}$ |
| q | Electronic charge | coulomb |
| t | Thickness | μm |
| $v_1$ | Hall probe voltage | volt |
| $v_2$ | Hall probe voltage | volt |
| V | Voltage | volt |
| $V_H$ | Hall voltage or voltage imbalance | volt |
| W/L | Width/length ratio | |
| $\rho_o$ | Resistivity | volt-cm/amp |
| $\mu_n$ | Electron drift mobility | $cm^2/volt\text{-}sec$ |
| $\mu_p$ | Hole drift mobility | $cm^2/volt\text{-}sec$ |
| $\mu_n^*$ | Electron Hall mobility | $cm^2/volt\text{-}sec$ |
| $\mu_p^*$ | Hole Hall mobility | $cm^2/volt\text{-}sec$ |
| $\vec{\nabla}$ | grad | $cm^{-1}$ |

# 1. INTRODUCTION

The purpose of this thesis is to create and implement a new hybrid mesh generator for finite element analysis. The resulting mesh is used in the simulation of practical semiconductor devices which arise in the electronic industry. These devices could not be dealt with by the existing mesh generator in our simulation package. The hybrid mesh generation approach is a combination of two different schemes, viz., the Delaunay and regular triangulation. To the best of our knowledge, this is the first time in which two different schemes are combined and used in practical semiconductor simulation. Our procedure combines the simplicity and controllability of a regular triangulation with the flexibility of a Delaunay triangulation. We note that a Delaunay triangulation by itself can triangulate any practical polygonal regions. However, the number of nodes generated by this process is often significantly higher than a proper solution with given accuracy would require. This observation is one of the main motivations for considering our approach. We demonstrate the capabilities of our hybrid mesh generator by presenting simulation results on both a Hall plate device and a lateral magnetotransistor. The Hall plate device simulation is analogous to work we recently were asked to perform for a major sensor manufacturing company.

In recent years, a great amount of progress has been made in the area of solid state semiconductor electronics. New designs of solid state electronic devices contain more complex circuitry, perform more reliably,

occupy less die area and consume less power. Such designs are being realized and improved constantly. Rapid growth is experienced in all three aspects of signal processing systems, viz., the areas of input transducer, signal processor, and output transducer. Such progress allows wider applications of solid state semiconductor devices. The resulting performance/price ratio favors the conversion of traditional electromechanical systems to electronic ones and the integration of input transducer, signal processor and output transducer. In the near future more sophisticated signal processing systems based on solid state semiconductor devices are expected.

A better understanding of semiconductor device behavior is the key to further progress in semiconductor device development. Numerical device simulation based on a mathematical model can be used in the investigation of semiconductor device behavior. Device simulation can provide a unique insight into the functioning of devices by giving the distributions of various physical quantities in the interior of the device, a region which is not readily accessible for experimental measurement [1].

From the economic point of view, the design cycle of new semiconductor devices such as microelectronic transducers includes some time consuming and expensive trial and error steps. Device simulation can be used to reduce semiconductor device development and optimization cost substantially [2].

Numerical device simulation involves the numerical solution of the

basic semiconductor equations. The basic semiconductor equations consist of the Poisson's equation, the continuity equations for electrons and holes, and the current density equations for electrons and holes [2]. Various device simulation programs, such as the B2DE, FIELDAY and HFIELD have been reported in the literature [3, 4, 5, 6, 7, 8, 9]. None of them address the influence of the magnetic field on the semiconductor devices. The sensor research group at the University of Alberta has developed the package ALBERTINA and reported the first successful application of finite element method for the two-dimensional simulation of integrated magnetic field sensitive devices [10]. This package aims at solving the modified basic semiconductor equations that account for the influence of the Lorentz force [1, 11, 12]. The finite element method is used in the solution procedure for the modified basic semiconductor equations, a system of partial differential equations. One of the main advantages of the finite element method is the capability of handling complicated geometric device domains. In order to exploit this advantage, a mesh generator capable of describing an arbitrary polygonal device domain is required. The problem of formulating the necessary input data for the finite element analysis is often not trivial.

Based on a hybrid mesh generation approach, a mesh generator is implemented to provide the necessary input data for the application of a finite element method to solve the basic semiconductor equations. The mesh generator has been developed in a modular approach. It consists of three main modules which can be developed and tested separately. Mesh generation is commonly acknowledged to be an important and resource consuming part of finite element computation [13]. The solution accuracy of

a finite element analysis is not only affected by the device geometry, boundary conditions and material properties, but also the density of the mesh and distortion of individual element. The quality of mesh also affects the computation resources required and the convergence of the iterative solution steps [14]. A good finite element mesh is one that guarantees stable computation, fast convergence and minimum error. A mesh with hundreds of elements may still be generated manually with the provision of experience, time and patience. When the number of elements is large (in the order of thousands) an automatic mesh generator to provide fast, efficient and reproducible mesh generation is crucial.

According to surveys done by Simpson [15] and Thacker [13], a variety of mesh generation techniques for solving partial differential equations has been proposed and implemented. These mesh generation techniques are based on several distinct approaches. They include the curvilinear coordinate mapping, local mesh refinement, vertex triangulation mehod, boundary contraction method and modified quadtree representation.

The curvilinear coordinate mapping applies numerical techniques to define a one to one mapping between a complicated region to a simple one. Such mapping can be used to transform a simple, regular mesh to one with general shape [16]. The main disadvantage of this method is the requirement of an appropriate co-ordinates transformation which is similar to the construction of an irregular mesh [13].

The local mesh refinement approach starts with a coarse mesh and subdivides some of the elements in the given mesh to produce a finer one. Each element is tested to determine the next element to be refined and then subdivided. This process is carried out until the refinement criterion is no longer valid [17]. This method needs an initial mesh which has to be prepared manually or by other methods.

In the vertex triangulation method, the mesh vertices are distributed first, then a suitable triangulation is built to link the existing vertices to obtain the final mesh [18].

The boundary contraction method continues shrinking the domain by generating strips of elements along the boundary. This shrinking process is performed continuously until the remaining region is null [19, 20].

The modified quadtree representation uses a recursive subdivision process to a region or subregion by assigning the subregions into a complete quadrant or a cut quadrant [21].

For most of the above methods, a large amount of input data is required in order to handle a region with a complicated boundary. The amount of user input not only strongly depends on the complexity of the boundary but also on the requirement of control over element distribution.

In general, triangular mesh elements can approximate a complicated

planar boundary better than rectangles. Since there is a natural correspondence between the number of nodal points in an element and the number of terms required in the local polynomial approximation, triangular mesh elements are good compromise between flexibility and computational effort required. Based on these reasons most planar mesh generation techniques use triangular elements.

In order to input the neccessary geometry data of device domains and facilitate user interaction, an interactive graphic interface is required. Interactive graphics systems are particularly suited for finite element analysis because they provide excellent means for man/machine interaction and support high data rate on ouput for presentation. Furthermore, an interactive graphics system provides the potential for improving the quality and quantity of data preparation. We use the display, button, slider, panel, cursor and menu facilities provided by the SunView graphics interface to enhance the user interaction. The flexibility of the mesh modification module relies on these facilities. The visual feedback gives the capability of continuously monitoring the data structure and greatly reduces the task of error detection [22]. Graphic inspection can be used to establish the correctness and suitability of the mesh. A rigorous mesh verification algorithm in geometric terms is available to ensure the validity of mesh representation [23].

This thesis describes the problem definition, design and implementation of a new hybrid finite element mesh generation scheme. The hybrid mesh generator can efficiently triangulate device domains of

any arbitrary polygonal shape. A modular decomposition approach has been used to develop the mesh generator. The strategy of our approach is to identify some specific goals to be achieved by the mesh generator. The mesh generation problem is then decomposed into three submodules, viz., the device domain decomposition, hybrid triangulation, and mesh modification module as shown in Fig. 1.1. The module decomposition process is carried out for each submodule recursively as shown in Fig. 1.2. The lowest level of this modular hierarchy consists of various data manipulation routines which can access the data structures directly.

In chapter 2, we discuss the specific goals of mesh generation, a brief outline of the mesh generator, tradeoff considerations as well as the limitation of hybrid approach. The overall framework of the existing simulation package (ALBERTINA) is also described.

In chapter 3, we use the geometry data to decompose the device domains into smaller subdomains. Upon the completion of device domain decomposition, each resulting device subdomain will be in the shape of a convex polygon. The initial hybrid triangulation is then performed in each device subdomain. Special care has been taken to ensure the proper connection between adjacent device subdomains, particularly between the Delaunay triangulation and regular triangulation domains. The capabilities provided by the modification module are described. With minimum user intervention, the density and element distribution of the initial mesh can be modified to suit particular needs.

In chapter 4, a brief discussion of the finite element method which is used in our simulation package is presented. The basic semiconductor equations and boundary conditions for the analysis of the Hall plate devices are also included.

In chapter 5, we show a practical application of the mesh generator. We present a simulation case which has commercial value. We simulate and optimize Hall plate devices in a manner similar to the one that we were recently asked to do for a major company. This simulation work can not be dealt with easily by the previous mesh generator alone. We discuss the simulation strategy and optimization procedure involved. Plots of equipotential lines and current lines are included. Results from simulation of a lateral magnetotransistor are also included.

Various mesh examples are included in appendix A to demonstrate the capability of the hybrid mesh generator to handle various devices with complicated domain geometry and to illustrate also the limitations.

The hybrid mesh generator has been implemented in C on a Sun III workstation running the UNIX operating system. The SunView graphic interface is used to provide direct visual interaction. A layout of the screen view is provided in Fig. 1.3.

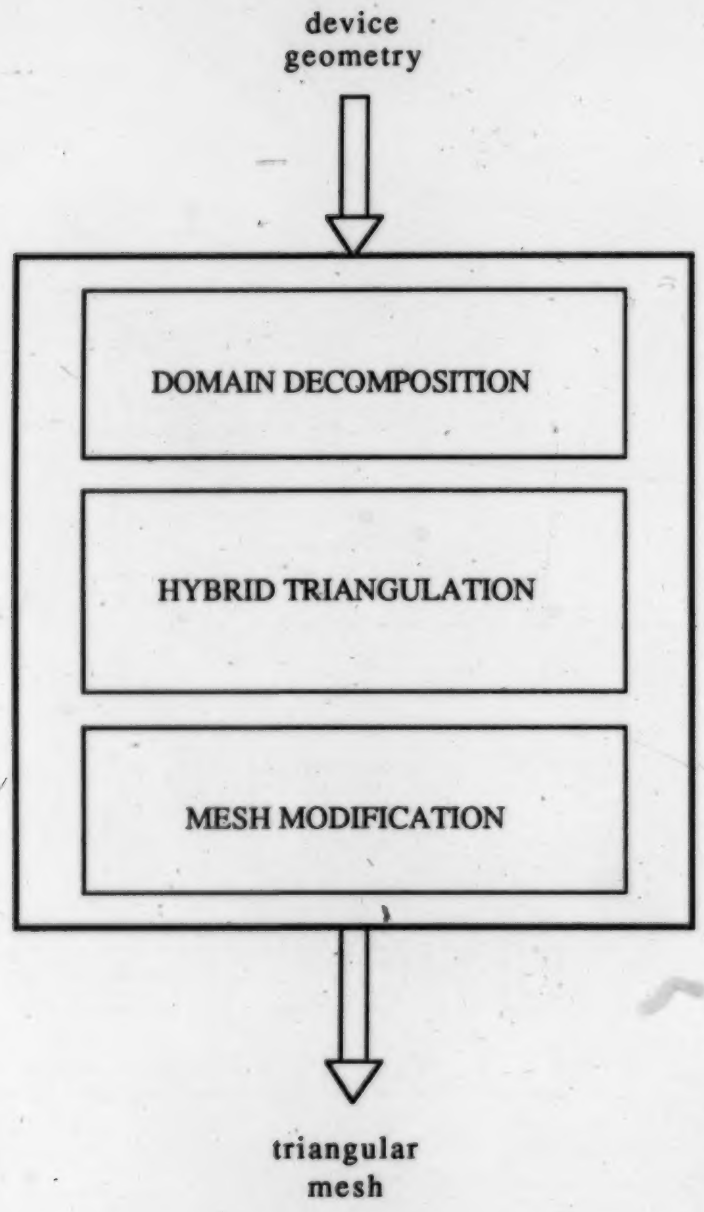


Fig. 1.1 Main modules of mesh generator

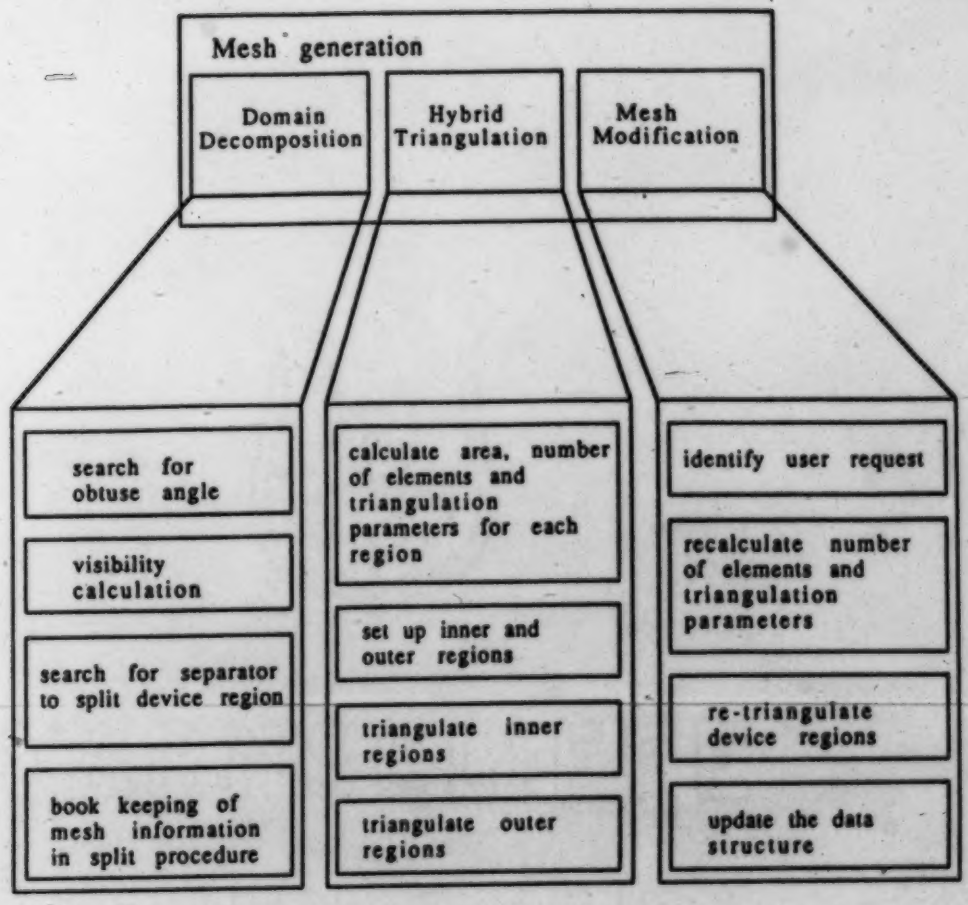
Mesh generation
Domain Decomposition
Hybrid Triangulation
Mesh Modification
search for obtuse angle
visibility calculation
search for separator to split device region
book keeping of mesh information in split procedure
calculate area, number of elements and triangulation parameters for each region
set up inner and outer regions
triangulate inner regions
triangulate outer regions
identify user request
recalculate number of elements and triangulation parameters
re-triangulate device regions
update the data structure

Fig. 1.2 Refinement of the mesh generation problem

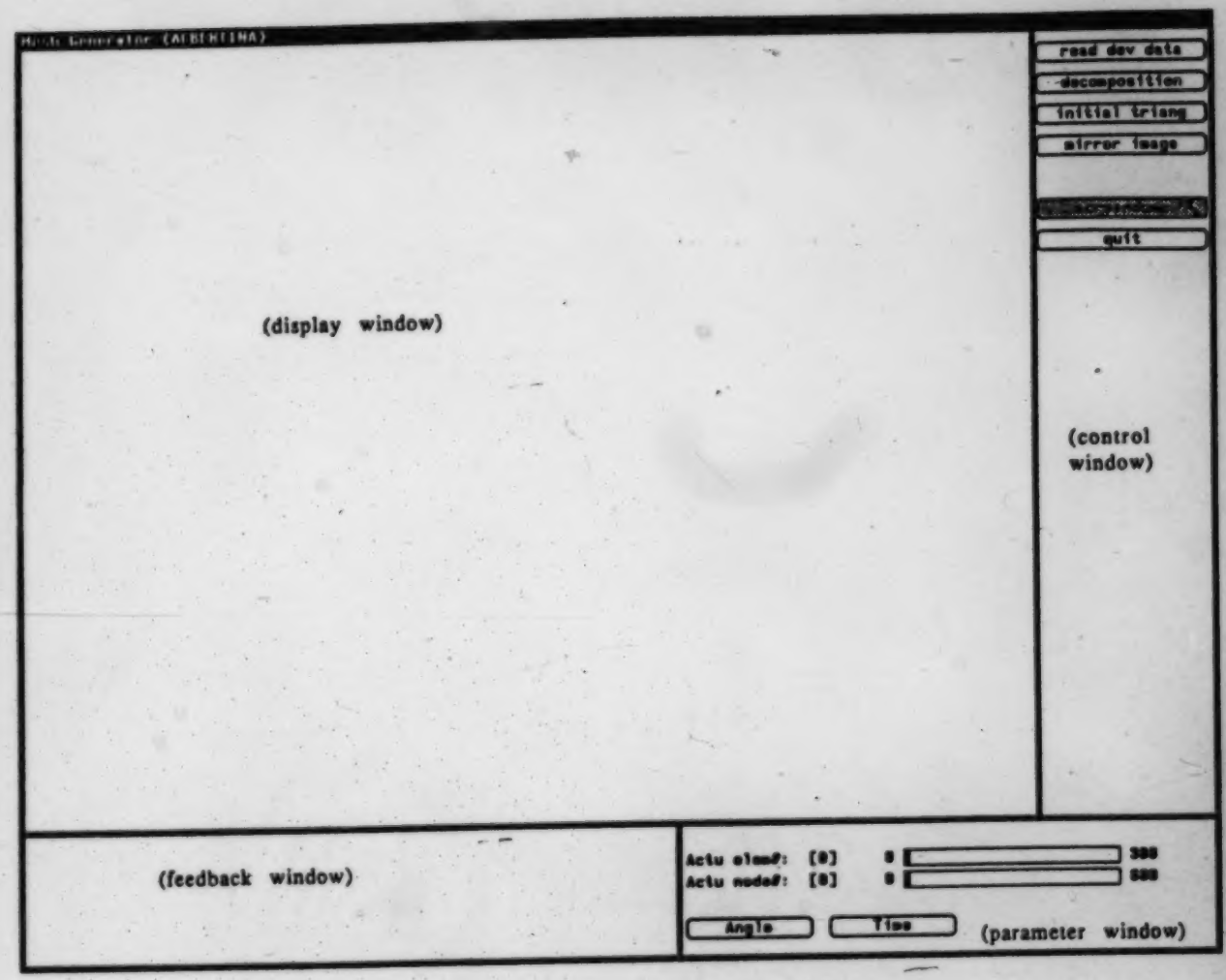


Fig. 1.3 Screen layout for mesh generator

# 2. CONCEPT OF HYBRID APPROACH

In this chapter we identify and discuss the objectives of finite element mesh generation. Our hybrid mesh generator is designed according to these objectives. We outline the advantages and disadvantages of both the regular and Delaunay triangulation and introduce the hybrid mesh generation approach as a compromise. The hybrid mesh generator is designed to be part of the ALBERTINA device simulation package. The overall hierarchy of ALBERTINA is included to show the connection between different modules. The data structure used in the mesh generation is discussed in the last section.

## 2.1 Objectives of Finite Element Mesh Generation

The primary goal of a finite element mesh generator is to partition a given domain into a finite number of elements, and provide the elemental, nodal and adjacency information to the partial differential equation (P.D.E.) solver to solve for unknown variables. The input to the mesh generator includes the domain geometry and the physical parameter of the semiconductor device.

We identify five objectives to be fulfiled by the hybrid mesh generator. They are as follows :

1. control the total number of elements
2. handle arbitrary polygonal boundary geometry
3. avoid extreme angles
4. avoid unnecessarily dense triangulation
5. control the mesh distribution.

The use of a denser mesh in the finite element analysis can result in a more accurate solution. However, in solving partial differential equations the dependence of the computational effort on the number of elements (or number of nodes) is linear at best. Usually this dependence approaches an exponential form. Most numerical packages, such as SPARSPAK [24], have an upper limit for the number of equations they can handle (e.g. approximately 3500 equations or 7000 elements on our system). If the package is run on a minicomputer, such as the Sun III system, the amount of core memory can restrict the number of elements and equations. The first objective is to allow the user to control the total number of elements to be generated over the device domain so that he can tailor the size of the simulation problem.

Our mesh generator is designed to be used as part of a semiconductor simulation package. Since semiconductor device geometry can assume a very complicated shape, the second objective states that the mesh generator should be able to handle device geometry of arbitrary polygonal shape. For instance the magnetic sensing devices can assume the shape of a cross, an octagon, or a rectangle which has large length to width ratio with long U-shape interfaces.

The error in applying the finite element method is greatest for extreme angles [25, 26, 27]. Mesh irregularity can affect the accuracy of finite element computation. The error in finite element analysis is in some cases inversely proportional to the smallest angle in the mesh [28]. Very acute angles can result in computational instability (in terms of convergence) [13]. Therefore, the third objective of the finite element mesh generation is to avoid extreme angles.

In various regions of a semiconductor device, the change of variables may vary in one direction only. The mesh generator should be able to avoid excessive use of mesh to cover a region in which a solution variable changes slowly. Objective four is to avoid the wastage of computational effort arising from such a source.

By referring to the initial simulation results, the user can adjust the mesh accordingly and repeat the simulation to obtain more accurate results. Objective five fulfils the requirement of interactive editing of the mesh so that the mesh density in a particular region, or an entire device domain can be altered.

## 2.2 Hybrid Mesh Generation Approach

In this thesis regular triangulation is referred to as the subdivision of a rectangular domain into a regular repetitive pattern of triangular elements. We follow the notation for a regular triangulation as in [27, 14]. We illustrate

the steps involved in regular triangulation with the example shown in Fig. 2.1. Start with a rectangular domain, the user specifies the number of horizontal and vertical triangulation strips, NH and NV respectively. The domain is subdivided into NH * NV smaller rectangular subdomains. Inside each subdomain, the diagonal splits it into two right-angled triangular element of equal size. The user can control the exact number of elements to be generated, i.e. 2 * NH * NV. We follow the triangulation and numbering algorithm described in [29] to generate the regular triangulation. The advantages of regular triangulation include : the controllability of number of elements and nodal distance, avoidance of obtuse angles and simplicity in implementation. Nodal distance is defined as the distance between neighbouring nodes. The main disadvantages of regular triangulation are the restriction to rectangular domains and that the resulting triangulation may contain extremely small interior angles. A typical regular triangulation is shown in Fig. 2.2. It contains seven horizontal strips, five vertical strips of element pairs and seventy triangular elements. In every element, one of the interior angle is much smaller than sixty degree.

For Delaunay triangulation, we subdivide a domain into triangular elements that are close to equilateral triangles. We follow the procedure used in [32]. First we calculate a triangulation size parameter H for each convex subdomain. We use the following relationship in the calculation of H : $A/n_e = H^2/2$, where A is the area of the subdomain, $n_e$ is the number of elements to be generated and H is the triangular size parameter. Then we shrink the boundary of the subdomain by H to produce an inner region. Then we apply

the quasi-uniform mesh generation algorithm [30] to triangulate inside the inner region. This results in a regular triangular pattern inside the inner region as shown in Fig. 2.3. Then we scan along the region between the inner and outer boundary and triangulate in a zig-zag manner. The resulting triangular elements along this strip are shown in Fig. 2.4. The circle criterion swapping algorithm in [25] is applied to the boundary layer to ensure the resulting triangulation is a Delaunay one, i.e. provide the most equiangular triangulation possible for a given set of points. The Delaunay triangulation can avoid extreme angles and fulfils the third objective identified in the previous section. Delaunay triangulation provides the flexibility of triangulating any convex polygonal region. However, Delaunay triangulation has the drawback of generating an excessive number of elements in regions where the change of a solution variable is in one direction only. The case as shown in Fig. 2.5 illustrates such an example. One of the inherent properties of Delaunay triangulation is the equidistance between adjacent nodes, i.e distances between neighbouring nodes are almost constant. For the same device domain shown in Fig. 2.2, Delaunay triangulation requires the use of 486 elements to cover the entire domain, and regular triangulation requires only 70 elements to obtain the same vertical nodal distance. The other disadvantage is that an element on the boundary layer can have an obtuse angle.

Both the Delaunay and regular triangulation possess advantages and disadvantages over each other. The mesh generation scheme developed in this thesis tries to combine them to extend the capabilities of mesh generation. Our mesh generator allows the user to choose the type of

triangulation in a rectangular domain and only Delaunay triangulation in general convex polygonal domains. While employing only Delaunay triangulation in convex polygonal domains, our mesh generator allows the user to choose the type of triangulation in rectangular domains.

Special care has been taken to ensure proper interconnection between elements in Delaunay and regular triangulation.

## 2.3 Albertina Framework : Overall Hierarchy

Albertina is a semiconductor device simulation package developed at our institution. It consists of a user interface, a geometry module, a physical parameter module, a mesh generator module and a partial differential equation solver module. From a user's point of view the framework can be depicted as in Fig. 2.6. The user interface is responsible for handling user interaction. Device simulation starts with the definition and manipulation of the geometric description of the device domain. This is handled by the geometry module which provides the necessary input geometry data for the mesh generation module. The user specifies the geometry and physical parameters through the user interface. The resulting device information is then stored in the data base. The user can then invoke the mesh generator which will use the device information in the data base as its input data. After the mesh has been generated, the global node and element number, element indices, nodal indices, and adjacency information are stored in four different files. The partial differential equations solver module reads in data from

these files and solves for a solution on the basis of the boundary conditions. The four modules are designed and implemented strictly adhering to modularity principles permitting separate design, implementation and testing of individual modules.

## 2.4 Data Structures for the Hybrid Mesh Generator

In this section, we discuss the data representation of device domains for decomposition and triangulation. The basic representation of a general triangular mesh includes the element, node and adjacency information [15].

In both the decomposition and triangulation stages the adjacency information is frequently referenced. The decomposition of device domain requires the introduction of a separator which involves nodal insertion. In order to facilitate the insertion of nodes onto the boundary of existing device subdomains, a circular doubly linked list is used to store the mesh information. The conceptual data structure of the circular doubly linked list is shown in Fig. 2.7. The doubly linked list structure can also accomodate the adjacency information effectively. The inner angle between any three consecutive nodes can be calculated without any search operation.

The conceptual doubly linked list is realized with a data structure which consists of three tables: the element table, element-node table and node table as shown in Fig. 2.8 and 2.9. Each entry in the element table corresponds to one device domain. The element table stores information about the number of

vertices (NUMV), first node (FIRST), triangulation type (TRITYP : 99 for Delaunay triangulation and 100 for regular triangulation) and number of triangles to be generated in a device domain (NUMT). The element-node table stores the information relating the element index and the node index. The element-node table stores the element index (ELEM), the node index (NODE), the index of the next node (PRO), the index of the previous node (PRE) and the index of the adjacent node (ADJ). The node table contains the coordinates of each node, with NX and NY representing the abscissa and ordinate values. In the three tables, I, J, and K are the element index, element-node index and node index respectively.

The data representations for a triangular mesh and a device domain are similar. The only difference is the absence of triangulation information such as the number of vertices (NUMV), type of triangulation (TRITYP) and number of triangles to be generated (NUMTRI). Examples illustrating data structures for both the device domain and triangular mesh are given in Fig. 2.8 and 2.9 respectively.

We name the index of the element table, the element-node table and the node table to be the element index, element-node index and the node index respectively. The element-node index of the first node of the first device domain is FIRST(1). The first node index of the first device domain is represented as NODE(FIRST(1)), and the corresponding x, y coordinates are NX(NODE(FIRST(1))) and NY(NODE(FIRST(1))). The adjacency information conveys both the adjacent element index and the adjacent node index. For example, in Fig. 2.8, the element-node index of the node adjacent to the node

with element-node index 1, is 11. The element index of the element adjacent to the element with element-node index 1, is 2.

This data structure is used in all three main modules of the hybrid mesh generator. With this simple data representation the mesh generator can be developed and maintained with less effort.

Rectangular device domain

Partitioning into rectangular subdomains

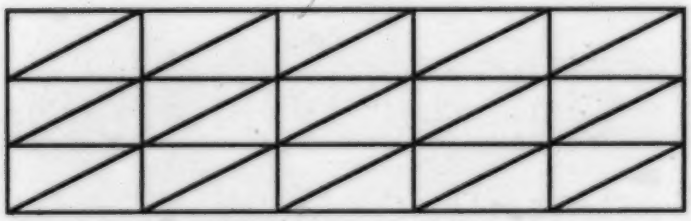

Regular triangulation with NV=5 NH=3

Fig. 2.1 Regular triangulation steps

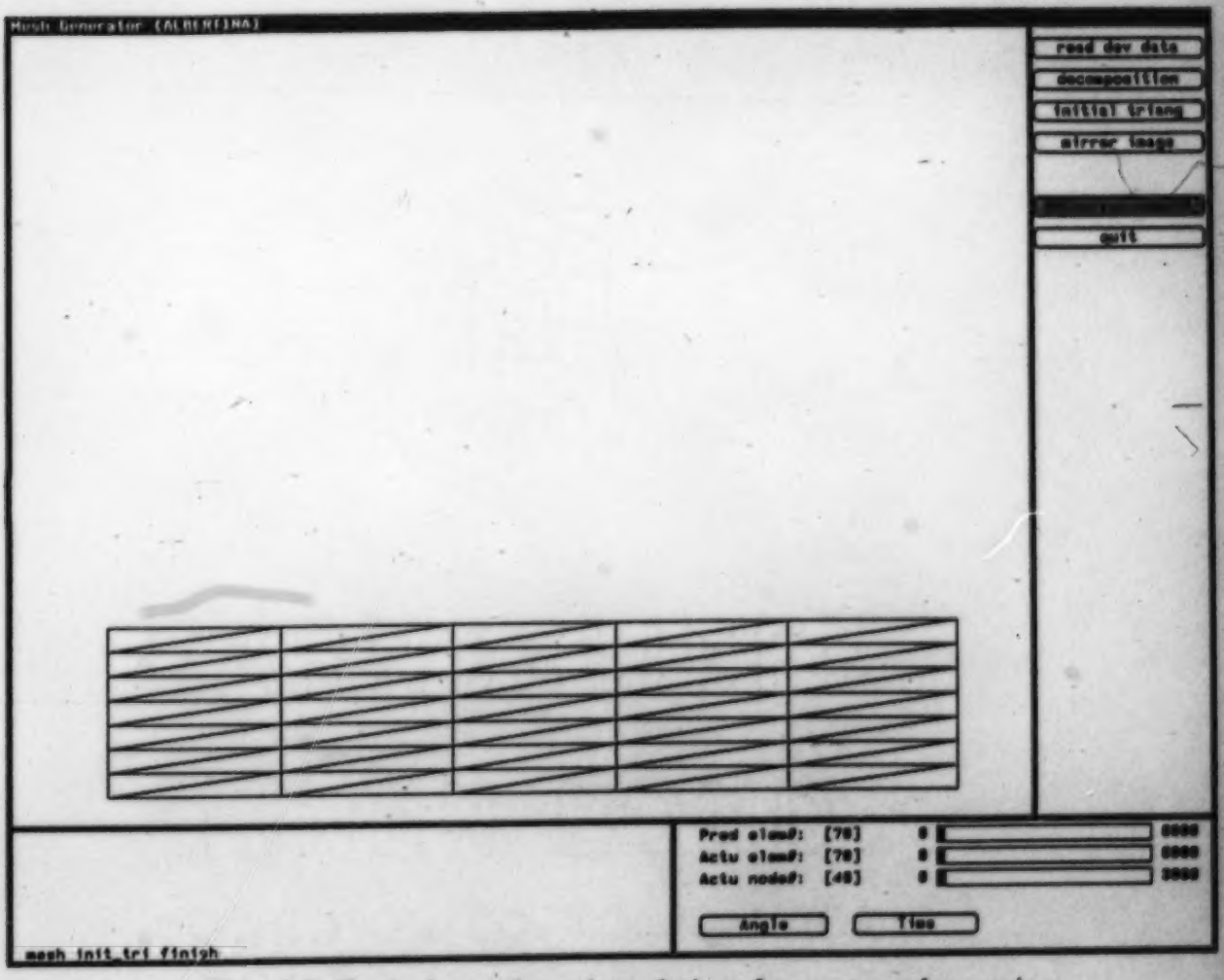


Fig. 2.2 Typical regular triangulation for rectangular region

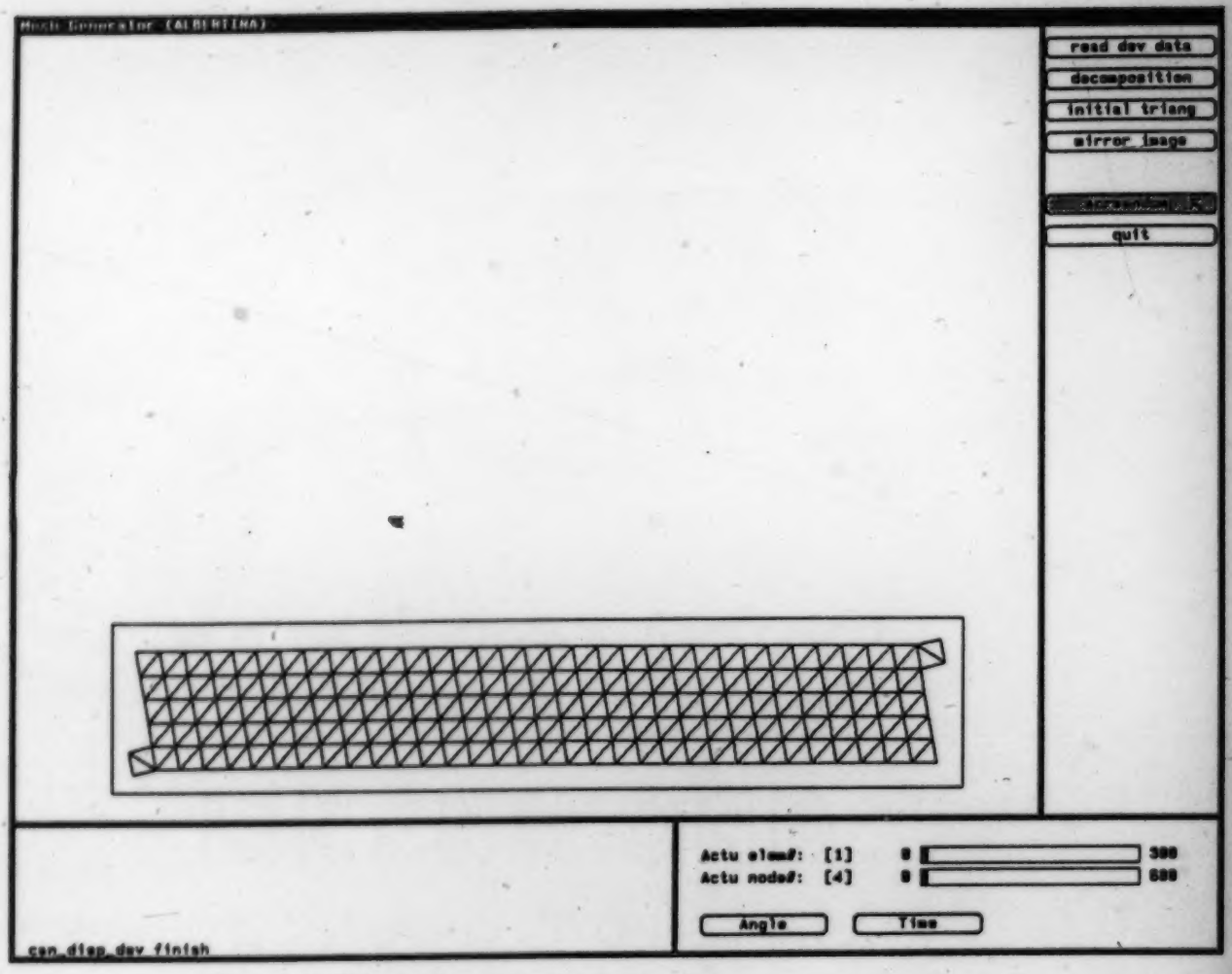


Fig. 2.3 Triangulate the inner region

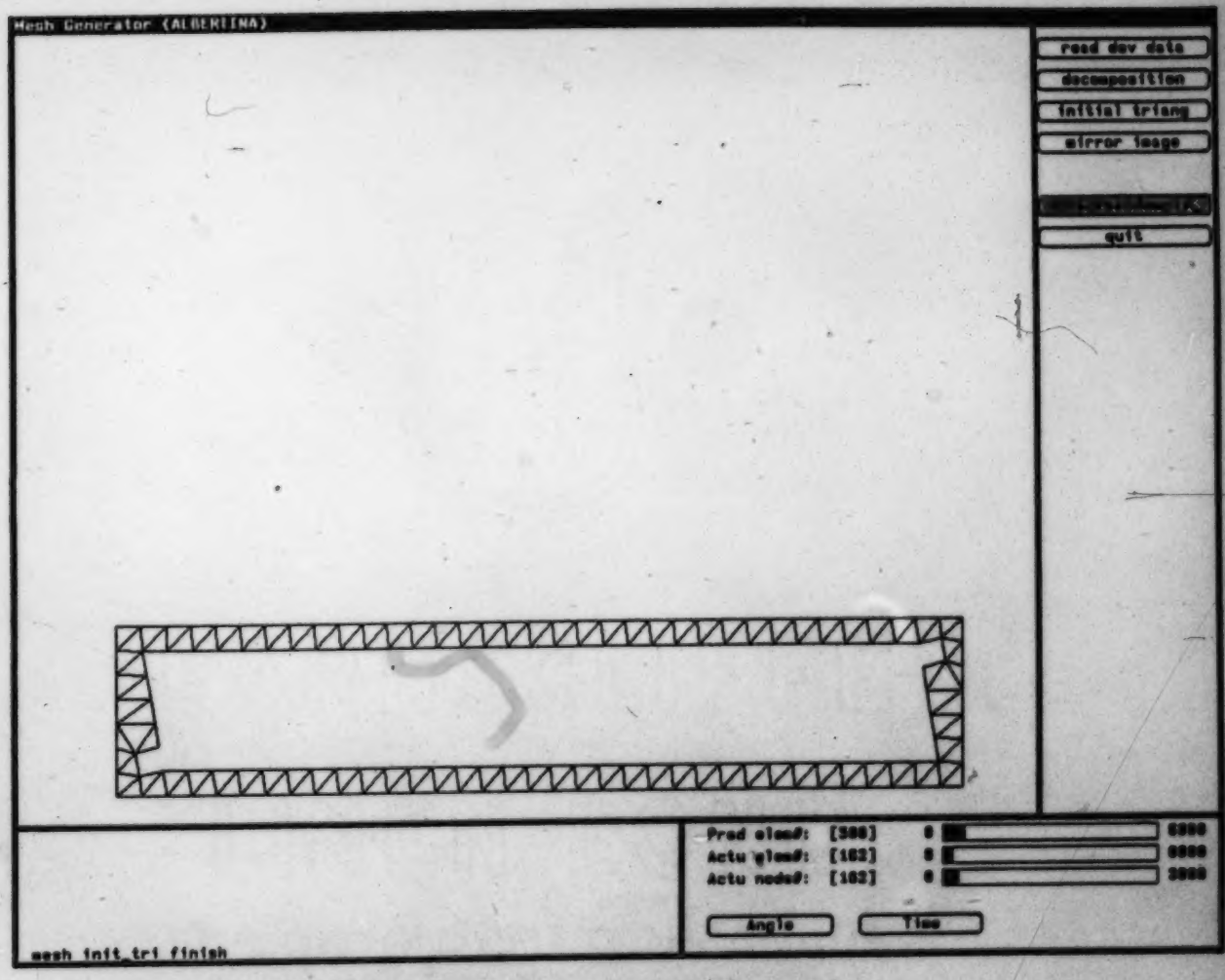


Fig. 2.4 Triangulate along the boundary strip

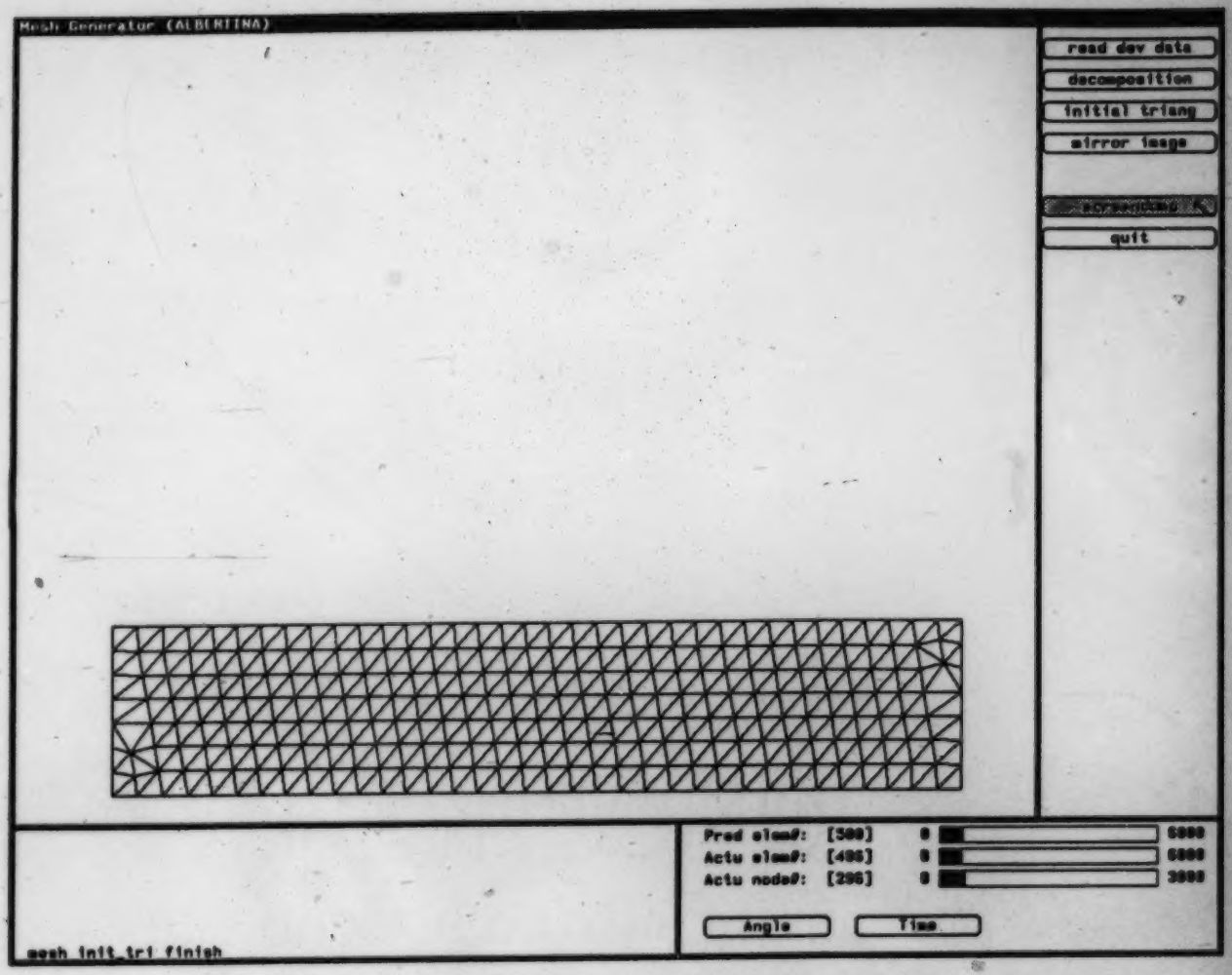


Fig. 2.5 Typical Delaunay triangulation for rectangular region

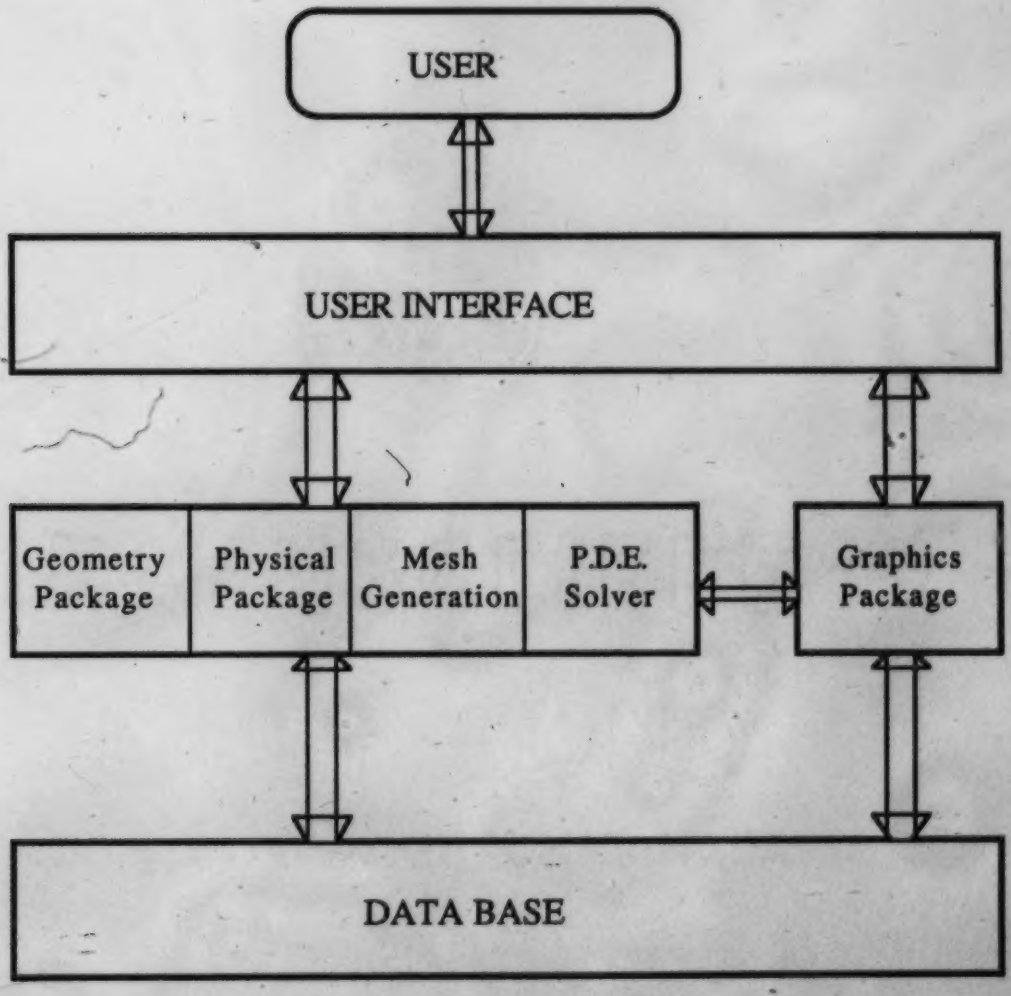


Fig. 2.6 User perception of ALBERTINA

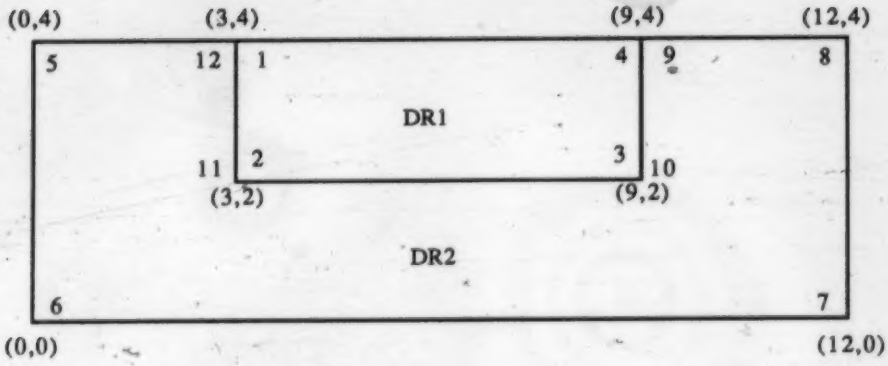


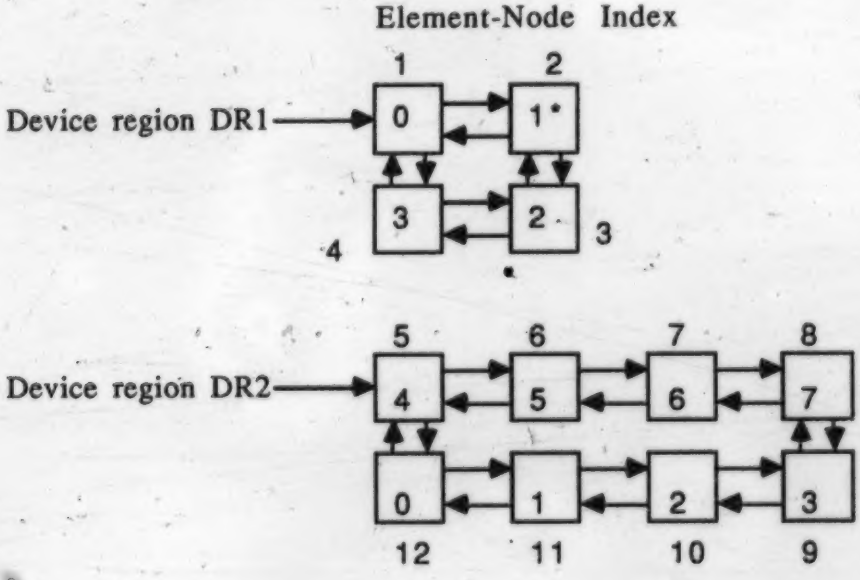


numbers inside square boxes are node indices (which do not appear in the above figure)

Fig. 2.7 Conceptual data structure of device domains

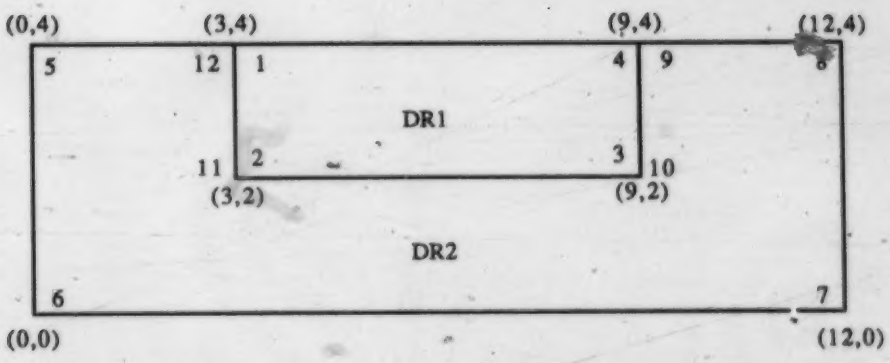


Element Table

| I | NUMV | FIRST | TRITYP | NUMT |
|---|---|---|---|---|
| 1 | 4 | 1 | 100 | 20 |
| 2 | 8 | 5 | 99 | 300 |

Node Table

| K | NX | NY |
|---|---|---|
| 0 | 3.0 | 4.0 |
| 1 | 3.0 | 2.0 |
| 2 | 9.0 | 2.0 |
| 3 | 9.0 | 4.0 |
| 4 | 0.0 | 4.0 |
| 5 | 0.0 | 0.0 |
| 6 | 12.0 | 0.0 |
| 7 | 12.0 | 4.0 |

Element-Node Table

| J | ELEM | NODE | PRO | PRE | ADJ |
|---|---|---|---|---|---|
| 1 | 1 | 0 | 2 | 4 | 11 |
| 2 | 1 | 1 | 3 | 1 | 10 |
| 3 | 1 | 2 | 4 | 2 | 9 |
| 4 | 1 | 3 | 1 | 3 | -1 |
| 5 | 2 | 4 | 6 | 12 | -1 |
| 6 | 2 | 5 | 7 | 5 | -1 |
| 7 | 2 | 6 | 8 | 6 | -1 |
| 8 | 2 | 7 | 9 | 7 | -1 |
| 9 | 2 | 3 | 10 | 8 | 3 |
| 10 | 2 | 2 | 11 | 9 | 2 |
| 11 | 2 | 1 | 12 | 10 | 1 |
| 12 | 2 | 0 | 5 | 11 | -1 |

observations : 1. node indices have been omitted
2. each node has its own (local) node index in each element

Fig. 2.8 Data representation for device domains

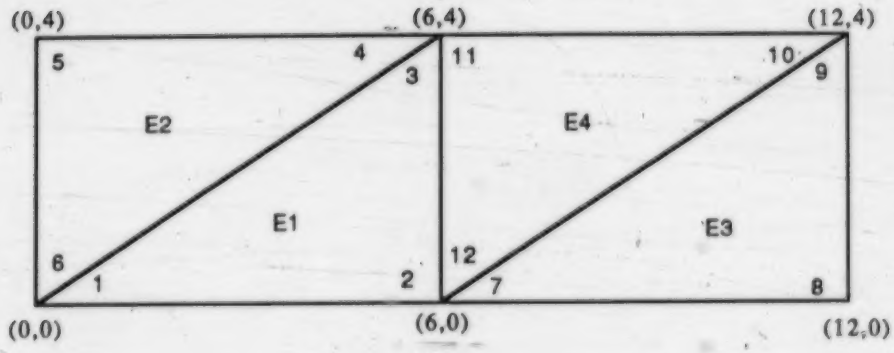


Element Table

| I | FIRST |
|---|---|
| 1 | 1 |
| 2 | 4 |
| 3 | 7 |
| 4 | 10 |

Node Table

| K | NX | NY |
|---|---|---|
| 0 | 0.0 | 0.0 |
| 1 | 6.0 | 0.0 |
| 2 | 12.0 | 0.0 |
| 3 | 0.0 | 4.0 |
| 4 | 6.0 | 4.0 |
| 5 | 12.0 | 4.0 |

Element-Node Table

| J | ELEM | NODE | PRO | PRE | ADJ |
|---|---|---|---|---|---|
| 1 | 1 | 0 | 2 | 3 | -1 |
| 2 | 1 | 1 | 3 | 1 | 11 |
| 3 | 1 | 4 | 1 | 2 | 6 |
| 4 | 2 | 4 | 5 | 6 | -1 |
| 5 | 2 | 3 | 6 | 4 | -1 |
| 6 | 2 | 0 | 4 | 5 | 3 |
| 7 | 3 | 1 | 8 | 9 | -1 |
| 8 | 3 | 2 | 9 | 7 | -1 |
| 9 | 3 | 5 | 7 | 8 | 12 |
| 10 | 4 | 5 | 11 | 12 | -1 |
| 11 | 4 | 4 | 12 | 10 | 2 |
| 12 | 4 | 1 | 10 | 11 | 9 |

Fig. 2.9 Data representation for triangular mesh

# 3. HYBRID MESH GENERATION

In this chapter, we discuss the initial and mesh modification stages of our mesh generation scheme, viz., region decomposition, initial triangulation and mesh modification. It is generally acknowledged that automatic triangulation for a convex polygon is much easier than for a general polygon. Considering this fact, the first step of our mesh generation scheme is to subdivide general polygonal domains into convex subdomains. This step fulfils the objectives of handling arbitrary device geometry and minimizing user intervention by automatic rather than manual subdivision. Upon completion of region decomposition, each subdomain will be in the shape of a convex polygon. Automatic mesh generation is then carried out inside each subregion according to the number of elements required and the specified triangulation type, Delaunay or regular. In this stage we basically follow the approaches proposed by Bykat [19] and Joe [30].

In section 3.1, we first discuss the procedures involved in the subdivision of device regions into convex subregions. Algorithms for automatic triangulation are discussed in section 3.2. The available mesh modification capabilities are presented in section 3.3.

## 3.1 Decomposition of Device Region

The device region decomposition algorithm described in this section

is applied to each device region. We use the device region $DR_3$ shown in Fig. 3.1 as an example throughout our discussion. In $DR_3$ there are four reflex vertices VR1, VR2, VR3 and VR4. We resolve these reflex vertices by introducing separators to split the region $DR_3$ into subregions. One end of each separator is always VR itself. In the general case, we scan through every vertex in every device region and apply the automatic region subdivision algorithm until all reflex vertices are resolved.

Consider the case for DR3, suppose we start scanning from the left upper corner of DR3 in a counter clockwise order, the first reflex vertex we will encounter is VR1. We modify Lee's algorithm [31] to calculate the visible boundary of DR3 from VR1. As shown in Fig. 3.2, the dotted lines indicate the visible parts of DR3 from VR1. Then we assign vertices along the visible boundary as candidates for the other end point of the separator. This is done based on the angle subscribed by each boundary. Vertices will be assigned for every visible portion that extends an angle of more than five degrees. The resulting vertices are shown in Fig. 3.3. The vertices inside the inner cone will then be considered as possible separator end point. If we use any vertices outside the inner cone, the resulting subregions may still contain the same number of reflex vertices, that is we have not resolved the reflex vertex. This is elaborated in Fig. 3.4. Once we have identified the possible vertices inside the inner cone, we sort them in ascending order according to their distance from VR1. We first attempt to find a separator from the closer half of this list of vertices. As soon as any one of them satisfies the following condition, it is selected as the end point of

the separator. To illustrate the condition we use V1 in Fig. 3.7 as an example. The line joining VR1 and V1 makes four angles with the boundary of the device region, viz., $\theta_{11}$, $\theta_{12}$, $\theta_{13}$ and $\theta_{14}$. If the minimum of these four angles is greater than forty five degrees then the line joining VR1 to V1 becomes the separator. If this search fails, the whole vertices list will be scanned. For each possible vertex Vi, we calculate the minimum angle $\theta_{min\ i}$ out of $\theta_{i1}$, $\theta_{i2}$, $\theta_{i3}$ and $\theta_{i4}$. The result will be a list of minimum angles ($\theta_{min\ 1}$, $\theta_{min\ 2}$, . . . ) for the vertices (V1, V2, ...). The largest of the minimum angles ($\theta_{min\ 1}$, $\theta_{min\ 2}$, . . . ) identifies the separator end point.

This scheme avoids introducing narrowings (see Fig. 3.6) or small angles to the device region. Based on the first searching scheme, higher priority is given to vertices closer to VR1, thus avoiding the introduction of narrowings as shown in Fig. 3.6. The second searching scheme ensures the success in identifying a separator and at the same time avoids the creation of small angles as compared to the existing angles.

As we can see in Fig. 3.8, when we try to resolve VR2, VR3 is chosen as the other end point of the separator. In this case two reflex vertices VR2 and VR3 are resolved by the introduction of separator S23. The separator S23 splits DR3 into two device regions DR3 and DR32. Upon completion of the region decomposition procedures, the resulting device regions are all convex polygongal subdomains as shown in Fig. 3.8.

## 3.2 Hybrid (Delaunay and Regular) Triangulation

The Hybrid triangulation scheme consists of two different triangulation schemes : Delaunay and regular triangulation. Regular triangulation is the simplest form of triangulation and it is restricted to triangulate inside the rectangular regions. The user specifies the number of vertical and horizontal triangulation strips in regular triangulation regions. Consider the device domain shown in Fig. 3.9, it consists of five subdomains. We can apply regular triangulation to the rectangular subdomain and Delaunay triangulation in the other four subdomains. In this case, we specify 11 vertical and 11 horizontal triangulation strips for regular triangulation. The resulting triangulation is shown in Fig. 3.10.

Various Delaunay triangulation algorithms have been proposed for different applications [26]. Our approach is based on the work done by Simpson and Joe [32] and the steps are as follows :

1. calculate a triangulation parameter H for each device domain based on the area and number of elements to be generated,
2. each domain is shrunk by a width of H giving an inner region inside the device domain,
3. the inner region is then triangulated with a quasi-uniform mesh to generate an equidistance mesh,
4. triangulation is then performed along the strip between

4. triangulation is then performed along the strip between the inner and outer boundary. This is done in a zigzag manner and using the Watson's swapping algorithm [25] to ensure the resulting triangulation is a Delaunay triangulation.

We follow this scheme to triangulate the four non-rectangular subdomains in Fig. 3.9. The resulting hybrid mesh is shown in Fig. 3.11.

## 3.3 Mesh Modification

In the previous section we discussed the mechanism of generating an initial mesh for any polygonal device domain. Users with minimal simulation package or mesh generator experience can follow the examples to obtain an initial mesh. The means to modify the initial mesh are available to the experienced user to tailor his need. In the simulation of most new semiconductor devices, an efficient initial mesh is difficult to generate a-priori. Based on user experience and intuition, an initial mesh can be prepared to solve for a preliminary solution. On the basis of this preliminary solution the user can modify the mesh to conform to the changes of the dependent variables. Hence some means to edit the initial mesh are incorporated in our hybrid mesh generator.

Upon completion of device decomposition, all resulting regions will be convex polygons. In this section the term subdomain is used to refer to these resulting convex polygons. There are three mesh modification functions

subdomain, viz., slider control of homogeneous mesh density, mouse button control of particular subdomain mesh density and mirroring button function to duplicate an existing mesh. The slider function pertains only to the Delaunay triangulation domains. This slider located inside the parameter window, controls the total number of elements after the initial mesh generation. After the user has specified a new number of elements for the entire deviee domain, the number of elements in each subdomain is calculated according to :

$$N_r/N_t = A_r/A_D,$$

where $N_r$ denotes the number of element in the subdomain,

$N_t$ denotes the total number of elements,

$A_r$ denotes the area of the subdomain,

$A_D$ denotes the total area of Delaunay triangulation.

With this rule, the resulting mesh will be homogeneous inside each Delaunay triangulation region. We demonstrate the mesh density control with the device geometry shown in Fig. 3.12. First we apply Delaunay triangulation to the entire device domain and then use the slider to increase and decrease the mesh density as shown in Fig. 3.13 and 3.14 respectively.

The user can also change the mesh density of an individual device domain or subdomain by pressing the left or right button on the mouse. The user simply locates the mouse cursor inside the domain to be modified and presses the left button to reduce the mesh density or the right button to increase the mesh density. In Fig. 3.15 we increase the mesh density of the

upper left subdomain and decrease the mesh density of the lower subdomain.

The geometry of many magnetic field sensitive devices possesses a line of symmetry. Consequently, we can take advantage of this fact by triangulating a portion of the device domain and mirroring it about the line of symmetry. This mirroring mechanism not only saves mesh generation time but also allows the user to check the correctness of simulation result for zero magnetic field. The user is supported with mirroring functions to mirror image device triangulations about the left-hand side, the right-hand side, the top or the bottom edge as shown in Fig. 3.16

With these capabilities the initial mesh can be modified to meet the needs of a more knowledgeable user. It provides the potential to generate meshes capable of improving the accuracy while reducing the simulation cost.

### 3.4 Achievement and Limitations

The hybrid mesh generator is incorporated into our Albertina semiconductor device simulation package. It fulfils the five objectives we set out for mesh generation. In all our mesh generation, the number of elements being generated is always within ±5% of the user specified number. With the decomposition procedure, our mesh generator can triangulate any arbitrary polygonal device domain. The user is given the choice to avoid extreme angle with Delaunay triangulation or control the nodal distance to

reduce the mesh density. The mesh modification mechanisms provide convenient means to edit the mesh.

One inherent limitation of the hybrid mesh generator is that regular triangulation is only feasible inside rectangular domain. This restriction forces the user to use Delaunay triangulation in most device domains, i.e. can not control the nodal distance in particular direction inside a convex polygonal domain. Furthermore, if the user changes the mesh density of a particular subdomain making the triangulation parameters between adjacent subdomains very different, then the boundary layer may contain elements with small angles as shown in Fig. 3.17.

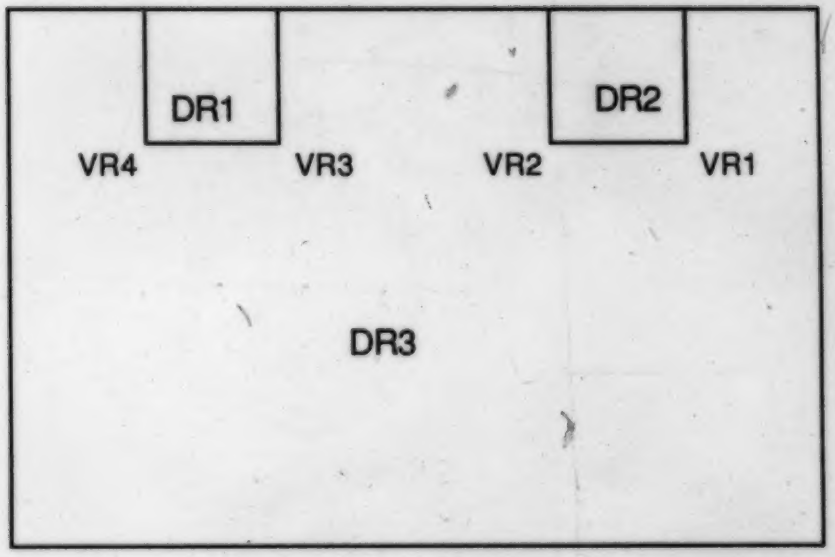


Fig. 3.1 Example of device domains with reflex vertices

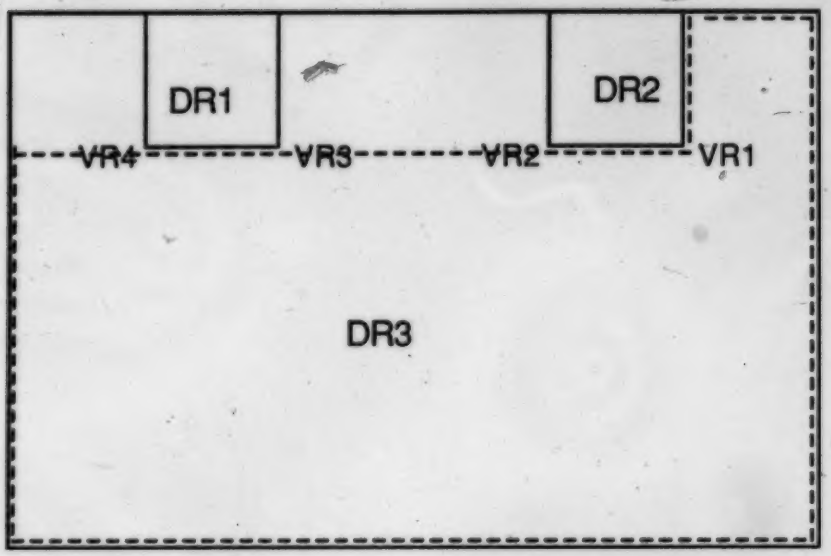


Fig. 3.2 Visible boundary from vertex VR1

(boundary with dotted line is visible)

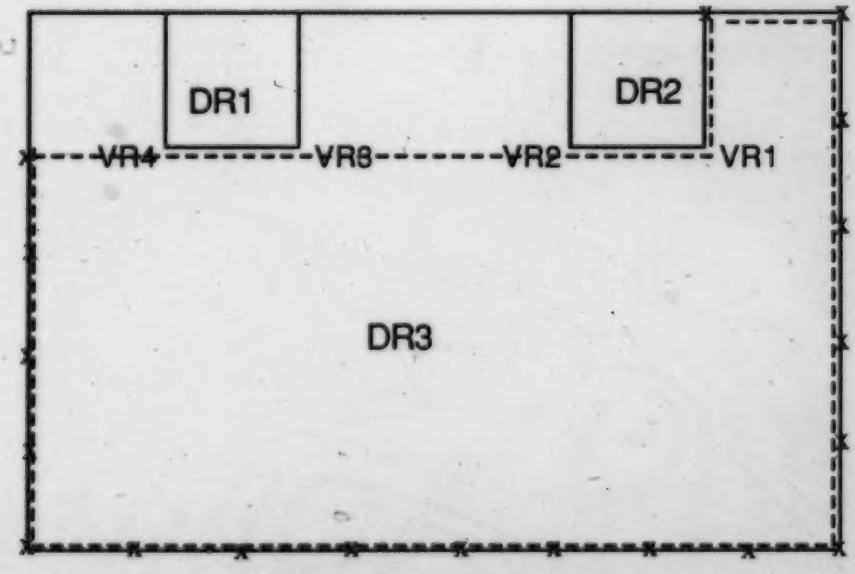


Fig. 3.3 Visible vertices from VR1

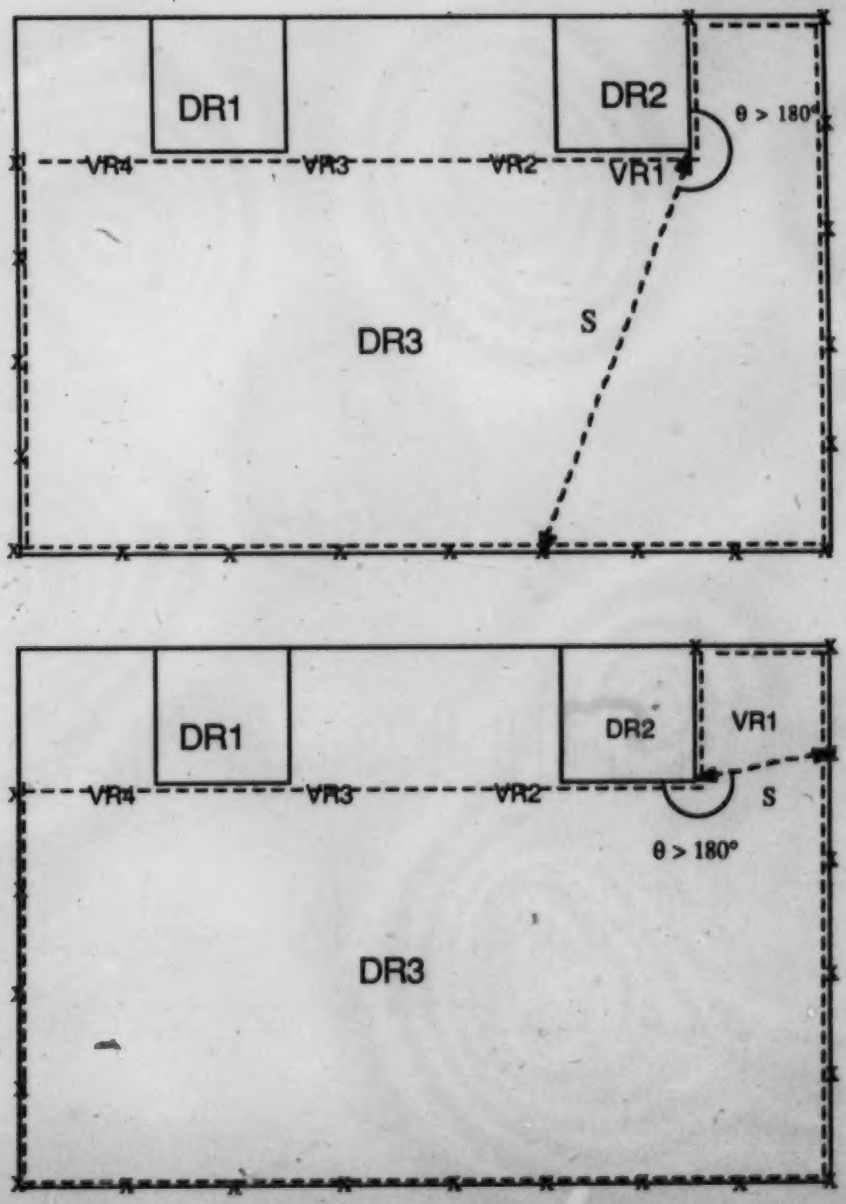


Fig. 3.4 Cases in which separator S fails to resolve reflex vertex VR1

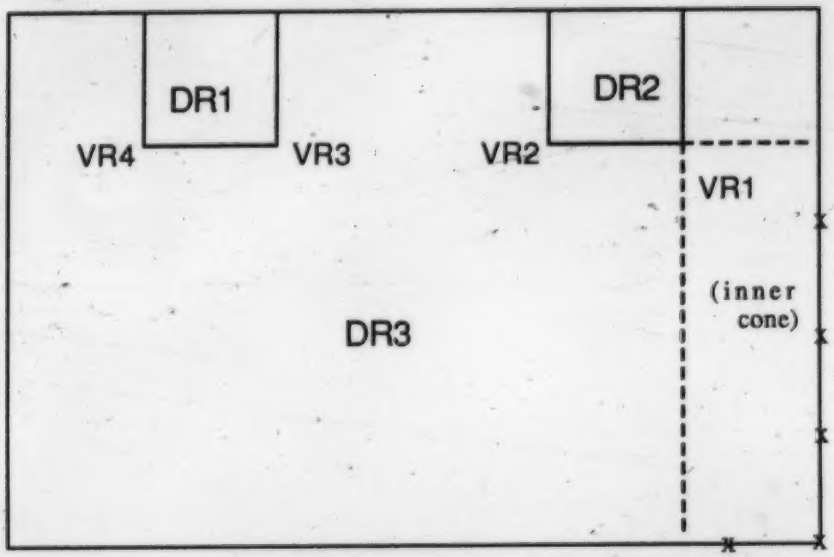


Fig. 3.5 Possible candidates of separator end points
(vertices inside inner cone)

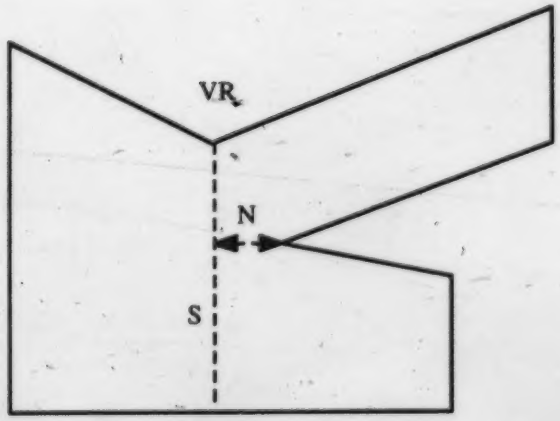


Fig. 3.6 Use separator S to resolve VR will introduce narrowing at N

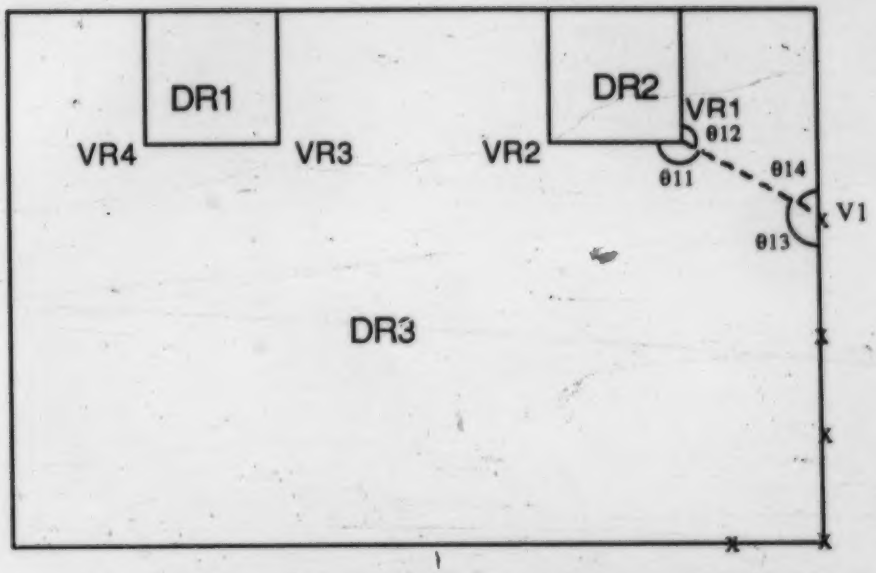


Fig. 3.7 Resulting interior angle of inserting a separator

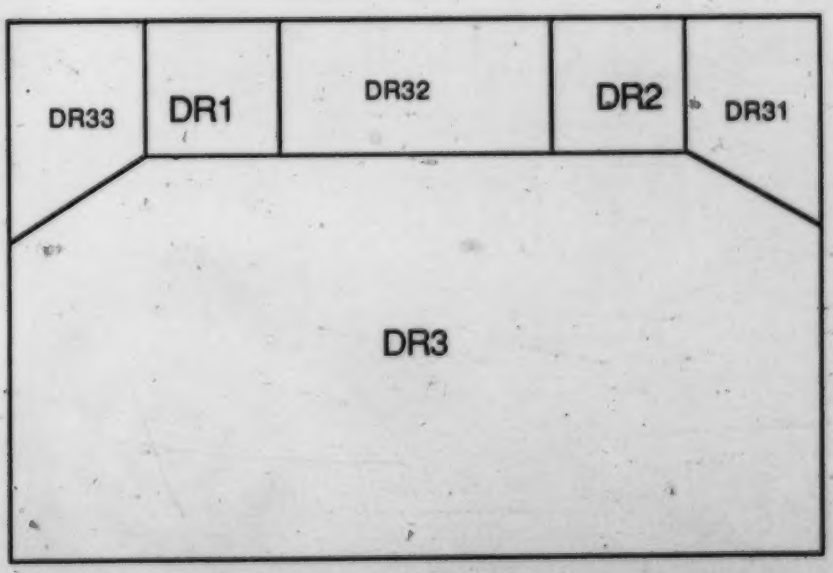


Fig. 3.8 Resulting device regions after decomposition

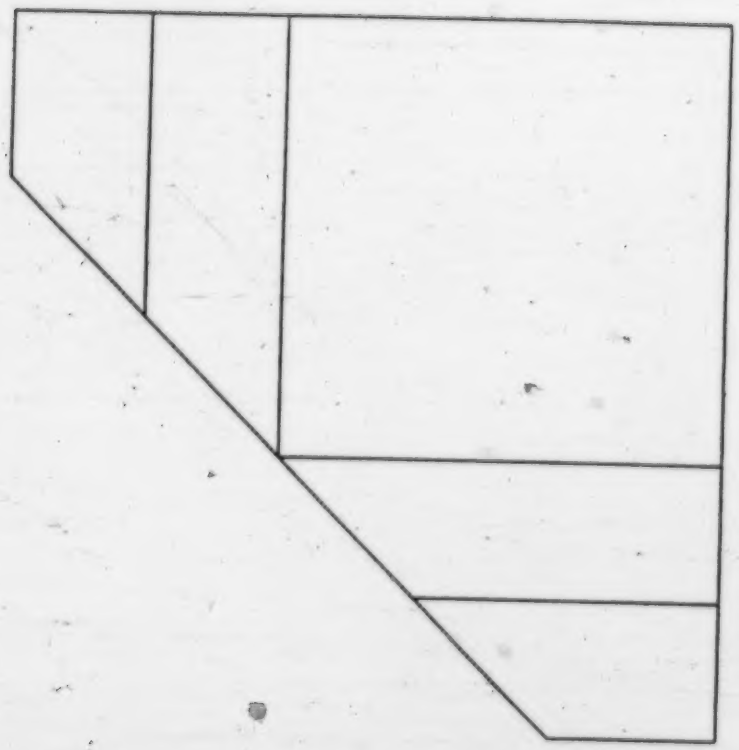

Fig. 3.9 Device geometry with five subdomains

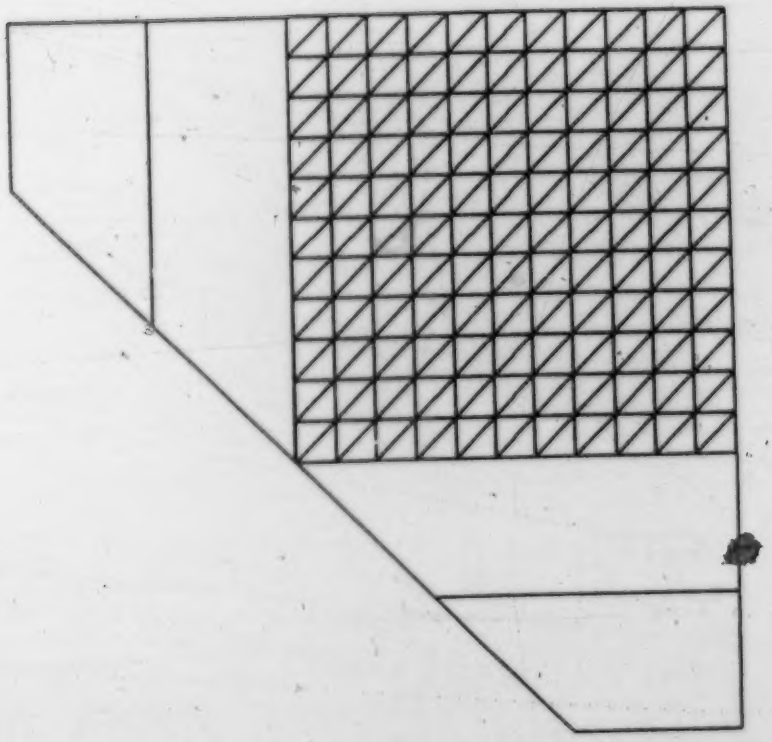

Fig. 3.10 Regular triangulation inside rectangular subdomain

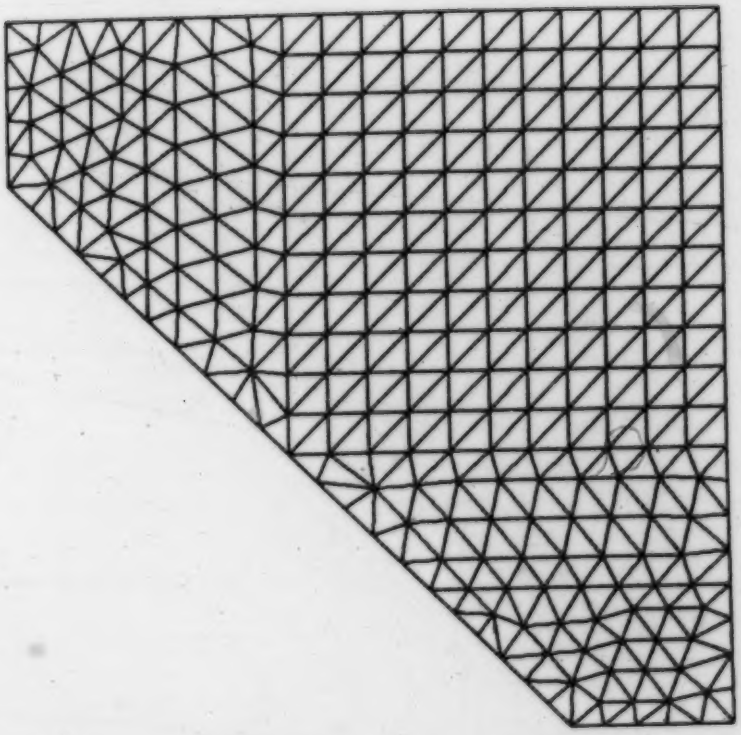

Fig. 3.11 Hybrid mesh of device with five subdomains

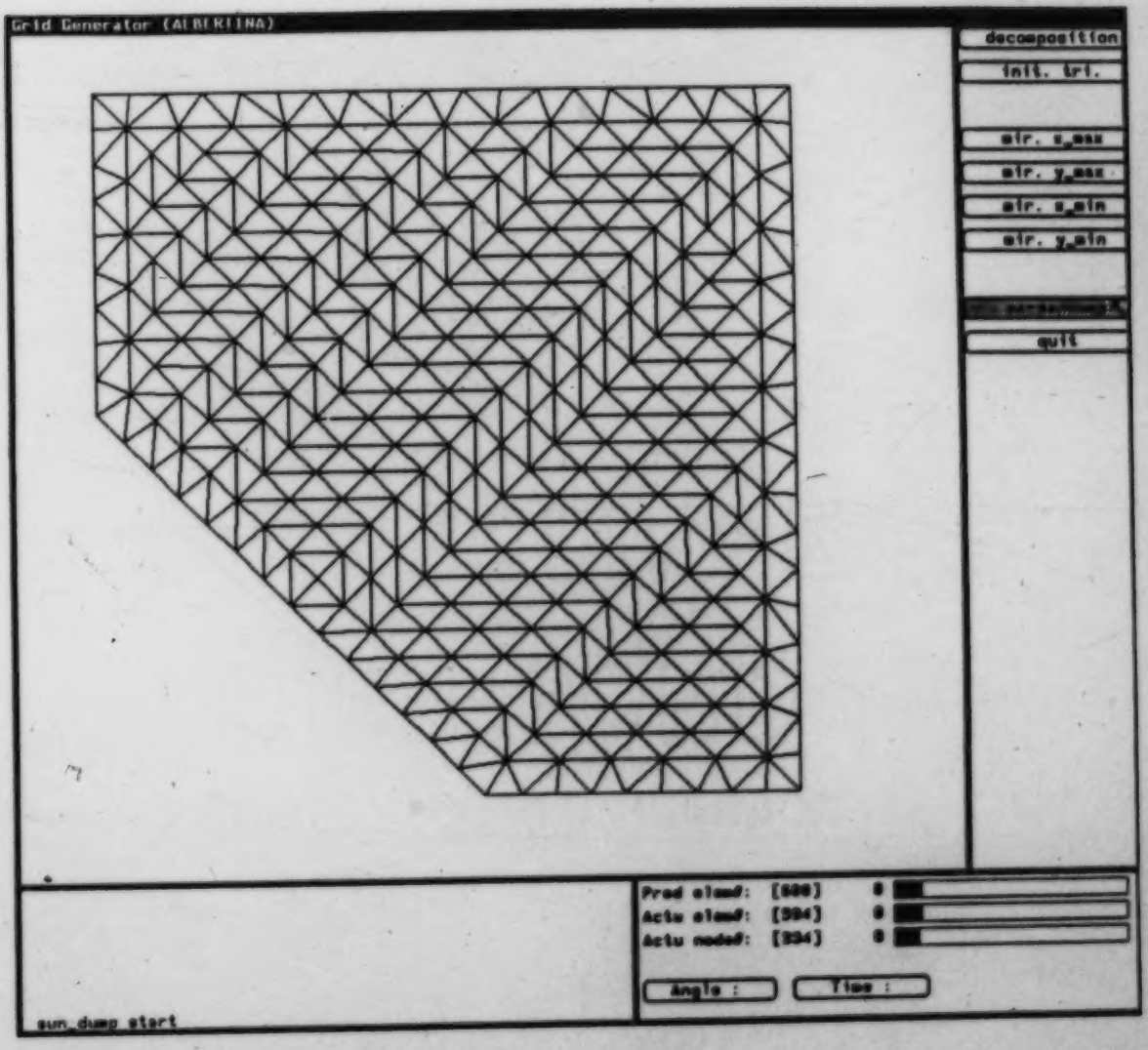


Fig. 3.12 Initial mesh with 594 elements

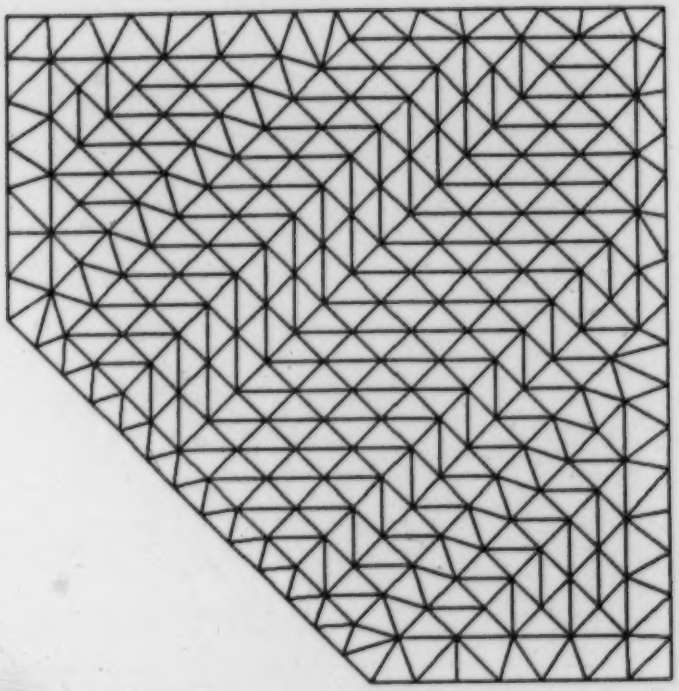

Fig. 3.13 Edited mesh with 448 elements

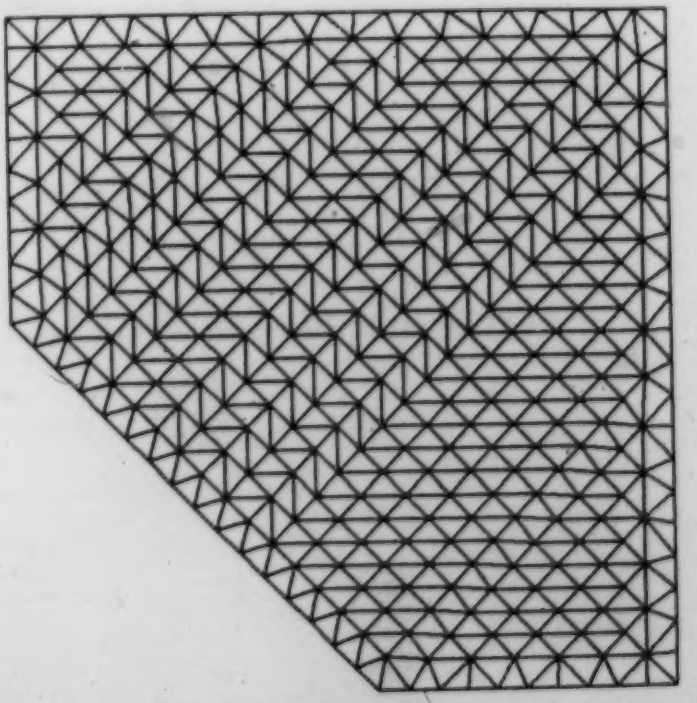

Fig. 3.14 Edited mesh with 748 elements

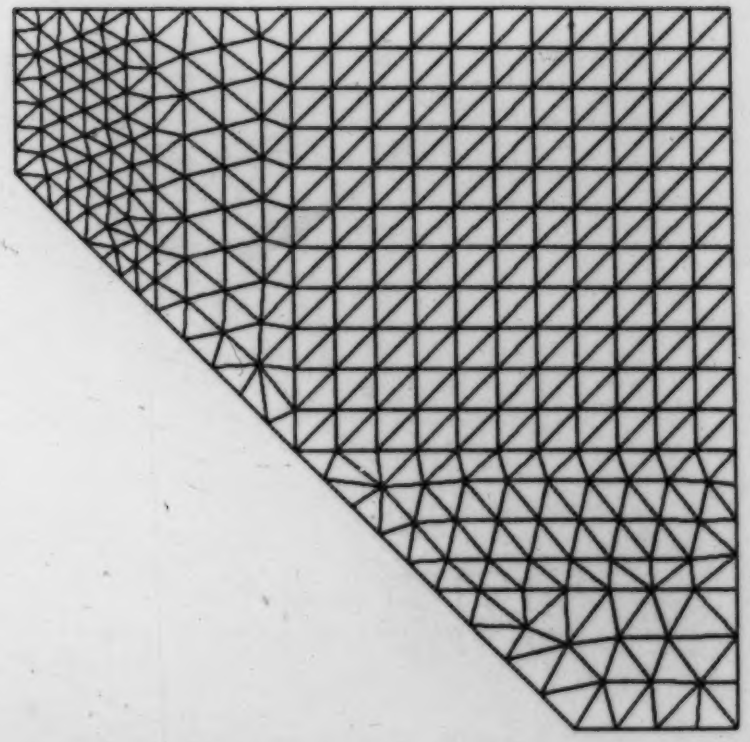

Fig. 3.15 Mesh with inhomogeneous mesh density

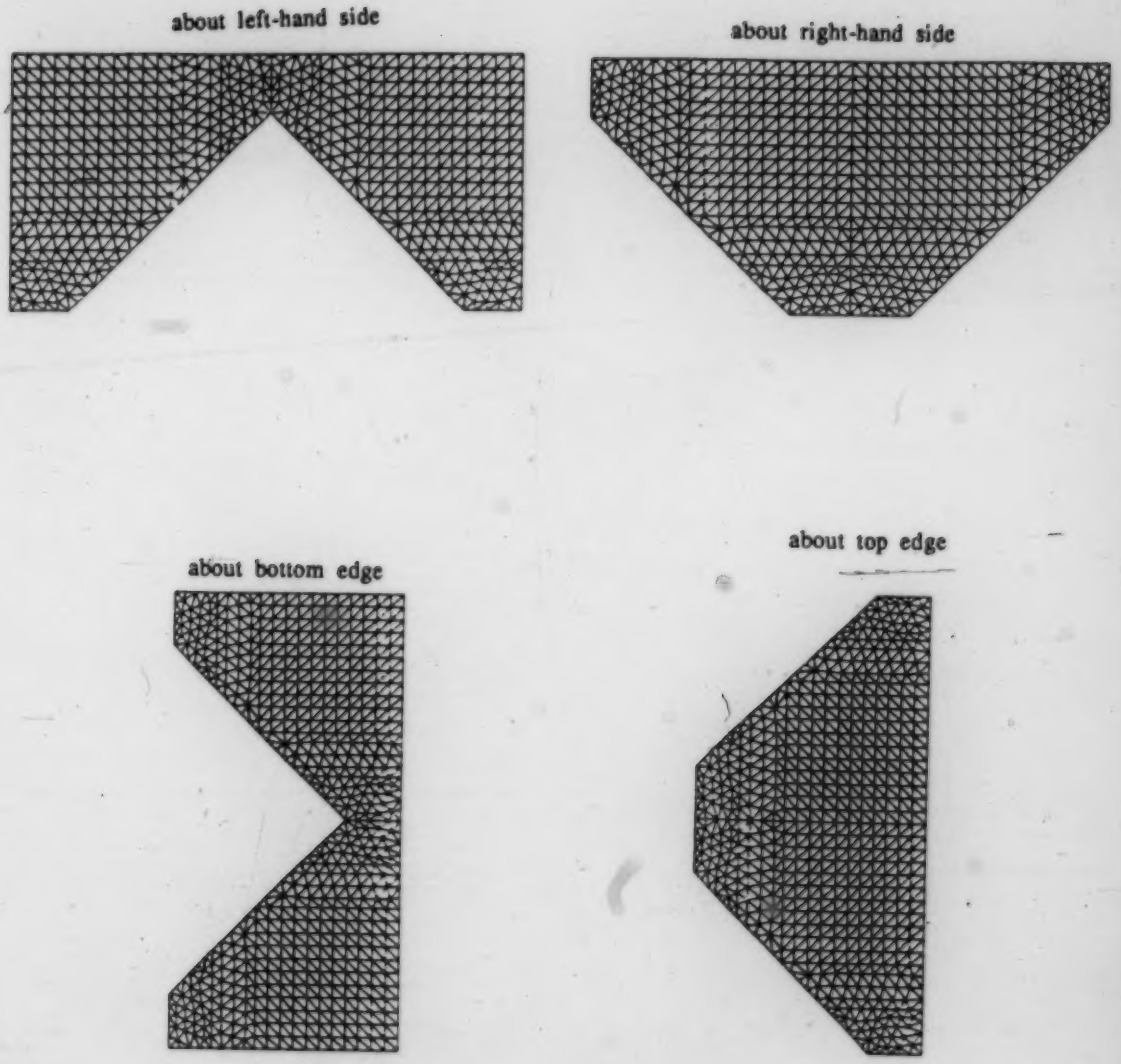


Fig. 3.16 Mirroring functions of mesh modification

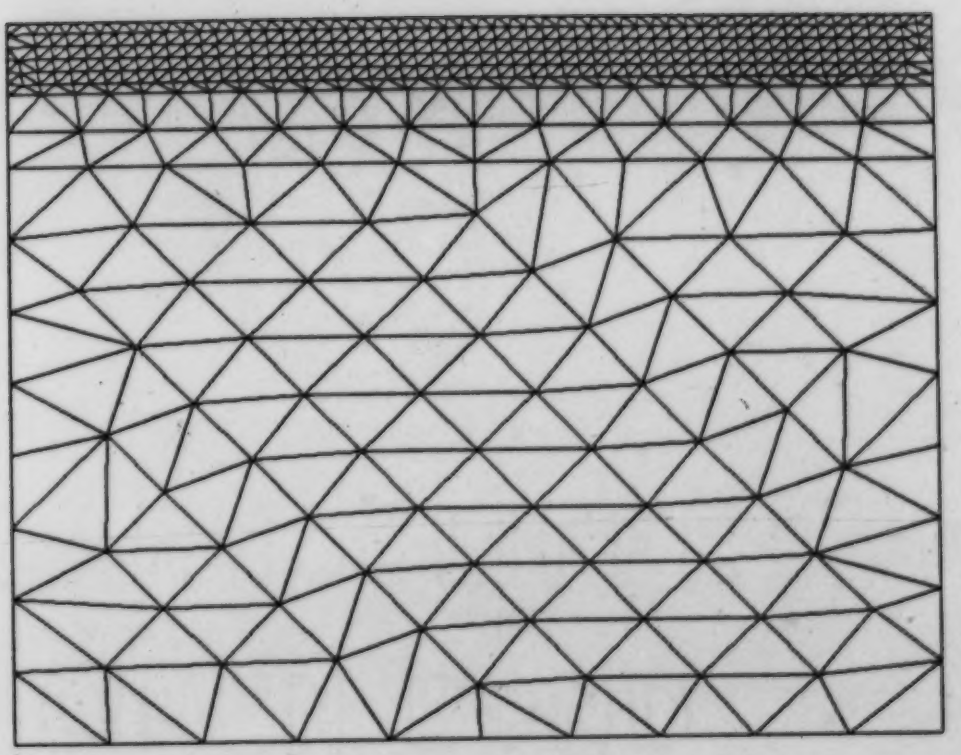

Fig. 3.17 Abrupt change in triangulation parameter

# 4. FINITE ELEMENT METHOD AND ANALYSIS OF HALL PLATES

In this section, the hybrid mesh generator is incorporated into a finite element analysis scheme which is used to solve the carrier transport equations for integrated semiconductor magnetic field sensors. We discuss the steps involved in the finite element analysis, the analysis of a semiconductor Hall plate device and the analysis of a lateral magnetotransistor. We formulate the system of equations governing the behavior of Hall plate devices as a basis for the simulation work. Results from the two simulation cases are included. In the Hall plate device analysis, only the Delaunay triangulation is used. In the lateral magnetotransistor simulation, the hybrid mesh scheme is used to divide the device domain.

## 4.1 Scheme of Finite Element Method

The finite element method is a powerful analysis technique for approximating the solution to partial differential equations. It has been successfully applied to the analysis of the Vertical Hall Device (VHD) and the MAGnetic Field Effect Transistor (MAGFET) [10].

The functional steps of the finite element method for simulating semiconductor devices include the following [33] :

1. define the device domain
2. divide the device domain into a finite number of elements

3. derive the elemental coefficient matrix for each element
4. assemble the global coefficient matrix from the elemental coefficient matrix
5. apply boundary conditions to the global matrix
6. solve the global matrix
7. display and interpret the results.

Mesh generation is essential to the second step of the above scheme.

## 4.2 Analysis of Hall Plate Devices

In this section the basic equations governing the behaviour of a Hall plate device under the influence of a weak magnetic field is presented. The boundary conditions required for the solution procedure are discussed. The techniqes involved in the calculation of Hall voltage of a particular Hall plate device with the geometry shown in Fig. 4.1 is outlined. This Hall plate device is sensitive to magnetic fields perpendicular to the plane of the device.

Based on the assumptions summarized in chapter 2 of reference [2], the current density equations under zero magnetic field can be expressed as follows :

$$\vec{J} = \vec{J}_n + \vec{J}_p \quad . \tag{4.1}$$

where

$$\vec{J}_n = q \cdot n \cdot \mu_n \cdot \vec{E} + q \cdot D_n \cdot \vec{\nabla}_n \tag{4.2}$$

$$\vec{J}_p = q \cdot p \cdot \mu_p \cdot \vec{E} - q \cdot D_p \cdot \vec{\nabla}_p \qquad (4.3)$$

Note that equations (4.2) and (4.3) include drift and diffusion components.

Under the influence of a weak magnetic field, the current density equations should be modified to assume the following form [30].

$$\vec{J}_n = (q \cdot n \cdot \mu_n \cdot \vec{E} + q \cdot D_n \cdot \vec{\nabla}_n) - \dot{\mu}_n \cdot (\vec{J}_n \times \vec{B}) \qquad (4.4)$$

$$\vec{J}_p = (q \cdot p \cdot \mu_p \cdot \vec{E} - q \cdot D_p \cdot \vec{\nabla}_p) + \dot{\mu}_p \cdot (\vec{J}_p \times \vec{B}) \qquad (4.5)$$

where

$(\vec{J}_n \times \vec{B})$ and $(\vec{J}_p \times \vec{B})$

come from the Lorentz force.

In the following derivation, we neglect diffusion current. The electron current equation under the influence of a weak magnetic field becomes :

$$\vec{J}_n = q \cdot n \cdot \mu_n \cdot \vec{E} - \dot{\mu}_n \cdot (\vec{J}_n \times \vec{B}) \qquad (4.6)$$

After some grouping and matrix manipulations, the equation becomes ;

$$\vec{J}_n = \frac{q \cdot n \cdot \mu_n \cdot \vec{E}}{1 + (\dot{\mu}_n \cdot B)^2} \begin{pmatrix} 1 & -\dot{\mu}_n B \\ \dot{\mu}_n B & 1 \end{pmatrix} \vec{E} . \qquad (4.7)$$

Since no injection of electrons or holes takes place, we can write ;

$$\text{div}\, \vec{J}_n = 0 , \qquad (4.8)$$

$$\operatorname{div}\left[\frac{q\cdot n\cdot \mu_n\cdot \vec{E}}{1+(\mu_n\cdot B)^2}\begin{pmatrix} 1 & -\mu_n B \\ \mu_n B & 1 \end{pmatrix}\vec{E}\right]=0\,, \qquad \text{with } \vec{E}=\begin{pmatrix}\frac{\partial V}{\partial x}\\ \frac{\partial V}{\partial y}\end{pmatrix}, \tag{4.9}$$

$$\operatorname{div}\left[\frac{\partial V}{\partial x}-\mu_n B\frac{\partial V}{\partial y},\ \mu_n B\frac{\partial V}{\partial x}+\frac{\partial V}{\partial y}\right]=0\,, \tag{4.10}$$

$$\frac{\partial^2 V}{\partial x^2}-\mu_n B\frac{\partial^2 V}{\partial x\partial y}+\mu_n B\frac{\partial^2 V}{\partial x\partial y}+\frac{\partial^2 V}{\partial y^2}=0\,, \tag{4.11}$$

$$\frac{\partial^2 V}{\partial x^2}+\frac{\partial^2 V}{\partial y^2}=0\,. \tag{4.12}$$

Observe that for a boundary with no electrode on it, the normal current component, as shown in Fig. 4.2, is zero, i.e.

$$\vec{J}_n\cdot\vec{n}=0 \tag{4.13}$$

where $\vec{n}$ is unit normal vector to boundary.

Substituting equation (4.7) for $\vec{J}_n$, equation (4.13) becomes

$$q\cdot n\cdot \mu_n\cdot \begin{pmatrix} 1 & -\mu_n B \\ \mu_n B & 1 \end{pmatrix}\begin{pmatrix}\frac{\partial V}{\partial x}\\ \frac{\partial V}{\partial y}\end{pmatrix}\cdot\vec{n}=0\,, \tag{4.14}$$

$$\left[\frac{\partial V}{\partial x} - \mu_n \dot{B}\frac{\partial V}{\partial y}, \mu_n \dot{B}\frac{\partial V}{\partial x} + \frac{\partial V}{\partial y}\right] \cdot \vec{n} = 0 . \qquad (4.15)$$

For electrode ab shown in Fig. 4.3, the outward normal current is obtained by integrating the dot product of the current density and the unit vector normal to the boundary. Specifically, for the eletrodes ab and cd in Fig. 4.3,

$$\text{outward normal current} = \int_{\text{electrode}} \vec{J} \cdot \vec{n} = \int_{x=a(c)}^{x=b(d)} q \cdot n \cdot \mu_n \left(\mu_n \dot{B}\frac{\partial V}{\partial x} + \frac{\partial V}{\partial y}\right) dx , \qquad (4.16)$$

and for the electrodes ef and gh,

$$\text{outward normal current} = \int_{\text{electrode}} \vec{J} \cdot \vec{n} = \int_{x=e(g)}^{x=f(h)} q \cdot n \cdot \mu_n \left(\frac{\partial V}{\partial x} - \mu_n \dot{B}\frac{\partial V}{\partial y}\right) dy . \qquad (4.17)$$

For the Hall probes, the leakage currents are set to zero. Since the problem is linear, we use superposition to calculate the voltage in the Hall plate device. We use $V_i(x,y)$, for i=1,2,3,4 to denote the voltage of the Hall plate device when we apply one volt to contact i and zero volts to the other contacts. The resulting equation is

$$V(x,y) = C_1V_1(x,y) + C_2V_2(x,y) + C_3V_3(x,y) + C_4V_4(x,y) . \qquad (4.17)$$

Since contact 1 is set at $V_o$ (5V), and contact 2 is set at $V_{gnd}$ (0V), equation (4.17) becomes,

$$V(x,y) = C_1V_1(x,y) + C_2V_2(x,y) + V_oV_3(x,y) . \qquad (4.18)$$

Substituting (4.18) back into equation (4.16) and (4.17), we obtain a system of simultaneous equations which has the following form

$$S_{11} C_1 + S_{21} C_2 = S_a ,$$

$$S_{12} C_1 + S_{22} C_2 = S_b .$$

From this system of equations, the Hall voltage (C1 - C2) can be determined. Furthermore, the conservation of terminal currents can be used to check the accuracy and validity of the solution.

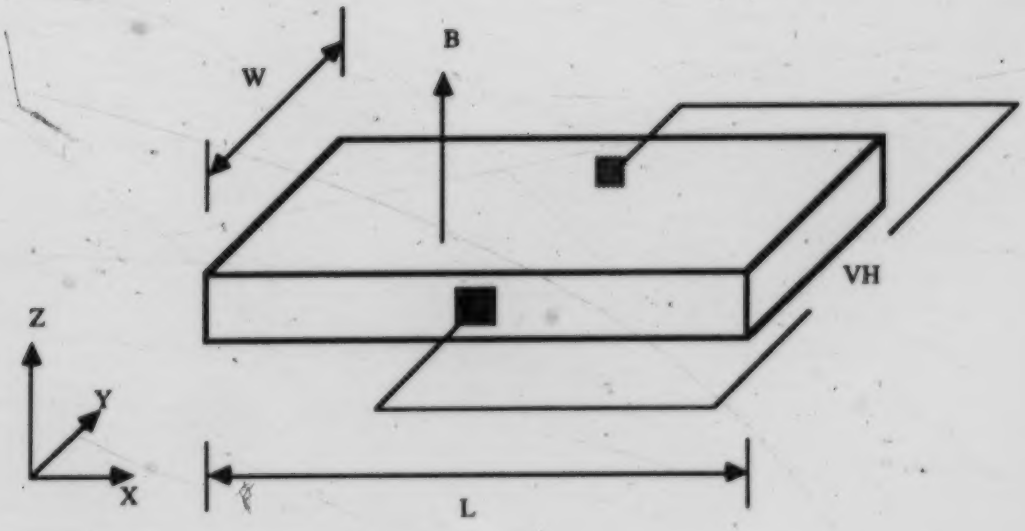


Fig. 4.1 Hall voltage in rectangular semiconductor sample

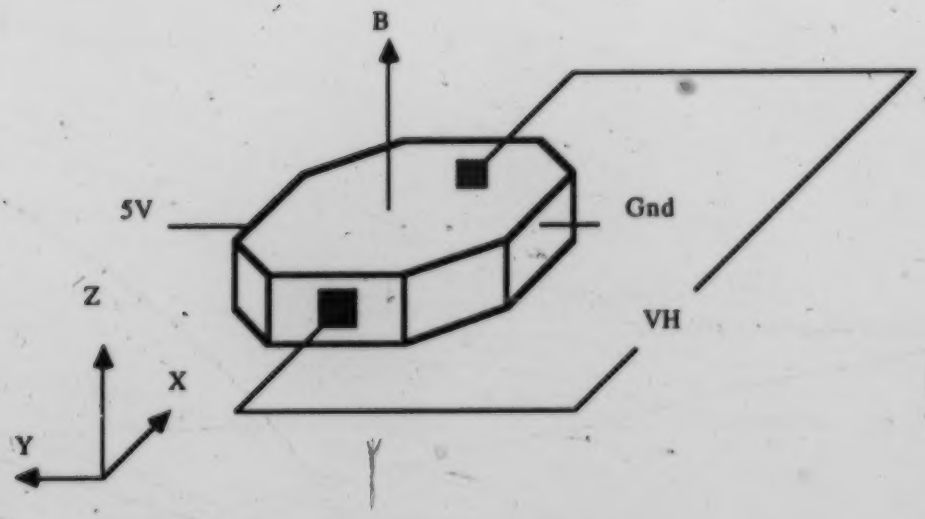


Fig. 4.2 Hall plate device in the shape of an octagon

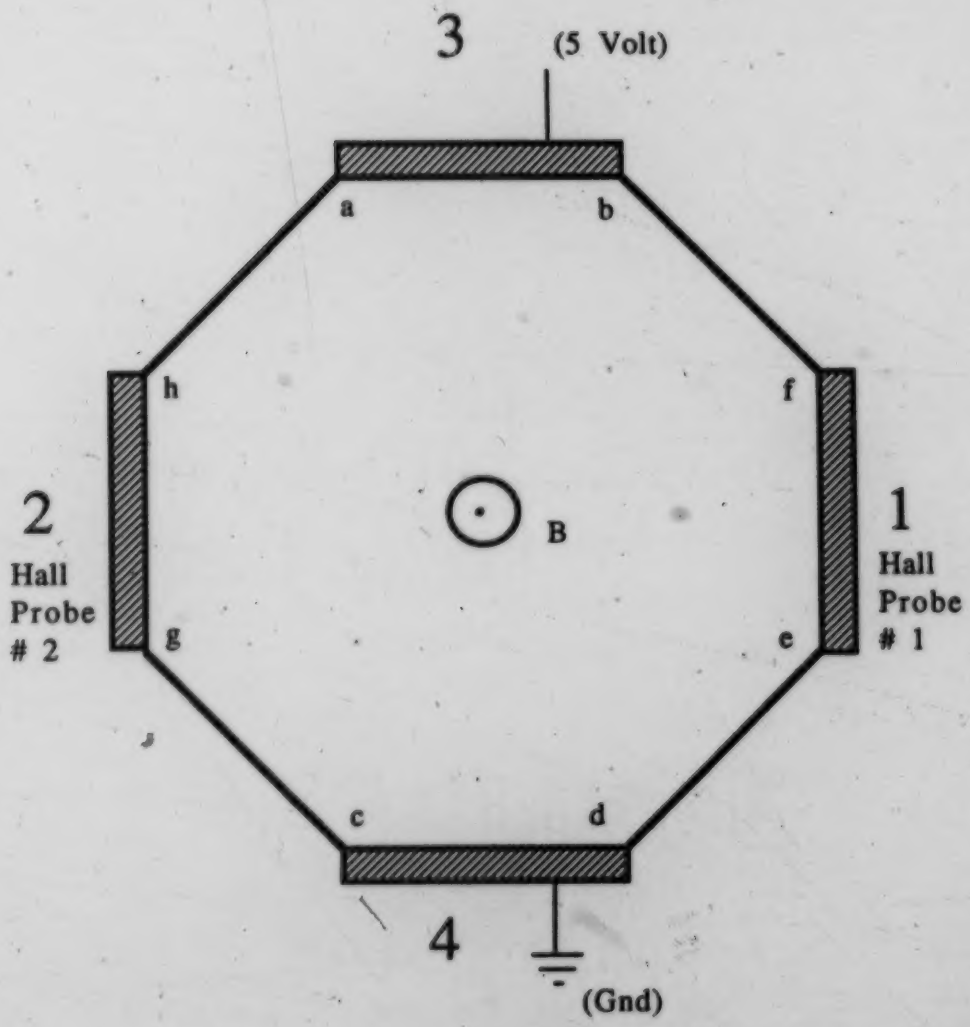


Fig. 4.3 Top view of Hall plate device with contacts

# 5. RESULTS: A CASE OF COMMERCIAL APPLICATION

As we have pointed out in the introduction, one of the main reasons to develop computer-aided design packages for device simulation is to reduce the time and cost of sensor design and development. The usefulness of a device simulation package can best be judged by actual simulation work. We successfully applied our simulation package with the hybrid mesh generator to simulate and optimize the Hall plate devices for a major sensor manufacturing company. In the first round, we simulated nine designs of different device geometry. After receiving the results from the first round, the designer from the sensor company requested for another round of simulations consisting of eighty one samples. We managed to simulate all eighty one samples in ten working days. The work entailed the preparation of different meshes, compilation of input data files, invoking the simulation package and evaluating the results. In section 5.1 and 5.2 we describe and present the strategy and typical results of the simulation. In section 5.3 the mesh and simulation results for a lateral magnetotransistor is included.

## 5.1 Simulation Strategy for Hall Plate Devices

The purpose of this simulation project is to optimize Hall plate devices in terms of the output Hall voltage vs. the effective length/width ratio. The first step in the simulation work is data preparation. According to the typical device geometry shown in Fig. 5.1, we set up a preprocessing program to prepare data files for the mesh and partial differential equation

solver. Since we use the same device and physical parameters for all the samples, the only input data required are the geometry parameters C and D, and the type of geometry setup as shown in Fig. 5.2. We were asked to use four different types of geometry setups, viz., type A, B, C and D. Type A is for a homogeneous mesh distribution throughout the entire device domain. Type B, C and D geometry setups partition the device domain into smaller subdomains so that the user can edit the mesh density of a particular subdomain interactively. In fact all samples are symmetric about their horizontal and vertical bisectors. In preparing the geometry data, we only input the part inside the third quadrant and then mirror the mesh both along the x and y direction to obtain the triangulation for the whole device. The steps involved are shown in Fig. 5.3. The resulting perfect symmetry allows us to check more accurately the operating conditions of the devices, under zero magnetic field.

For the examples shown below, we use a doping concentration of $2*10^{15}$ $cm^{-3}$, a device thickness of 5.35 $\mu$m, an electron mobility of 1545 $cm^2$/volt-sec and a magnetic field strength of 0.01 Tesla. We record the inward current into the 5-volt contact and the resulting Hall voltage, which is the potential difference between the two probes.

The device geometry is not rectangular, hence an effective length/width ratio is calculated with the following formula :

$$\text{Effective } L/W = V_{applied} / (I_{total} * \rho / t),$$

where $V_{applied} = 5.0$ volt,

$I_{total}$ = inward current into 5-volt contact,

$\rho = (q \mu N_D)^{-1}$ with $q = 1.6 * 10^{-19}$ C,

$\mu = 1545$ cm$^2$/volt-sec,

$N_D = 2 * 10^{15}$ cm$^{-3}$,

$t = 5.35 * 10^{6}$ m.

## 5.2 Simulation Results for Hall Plate Devices

The results on Hall voltage and terminal currents are recorded and tabulated. Table 5.1 shows the results of the first round of simulation. These results cover the cases in which the geometry parameters C and D are equal, i.e. for device geomtry that can fit into a rotated square. From Table 5.1, as the contacts becomes longer and longer the current flowing through the device increases directly. Refering to the plot in Fig. 5.4, the output Hall voltage depends on the size of the contacts and the Hall probes too. The maximum output Hall voltage ($V_H$=3.7mV) occurs at an effective length/width ratio of approximately 1.25. This effective length/width ratio correspondes approximately to the device geometry parameters of C=50 and D=50. Table 5.2 show the simulation results of the eighty one samples in the second round of simulation request. The results include geometry parameters (C, D), type of geometry setup, the contact current, potentials at Hall probes, output Hall voltage ($V_H$), and the effective length/width ratio (L/W) respectively. The plots of equipotential and current lines are shown

in Fig. 5.5 and 5.6 respectively. In the eqipotential lines plot, each step is 0.6 Volt. The potential of the Hall probe at the right hand side is only 3.36 mV higher than the one at the left hand side.

### 5.3 Mesh and Simulation Results for Lateral Magnetotransistor

We use our hybrid mesh generator to generate a mesh for the lateral magnetotransistor device shown in Fig. 5.7. Owing to the operating principle, the device is inherently extremely long, with a narrow U-shaped interface. In our case the length and width of the device are 150 μm and 10.7 μm respectively. In order to triangulate this long device domain, the application of Delaunay triangulation alone results in an extremely large number of elements (over 10000 elements). Consequently, we triangulate some subdomains with regular triangulation and with our hybrid scheme we cover the entire domain with 5258 elements and 2744 nodes. The mesh for the U-shaped interface and the base-emitter region is shown in Fig. 5.8. In this triangulation, we maintain a satisfactory nodal distance of 0.3 μm along the critical regions. The simulation results, the plots of equipotential and current lines, are included in Fig. 5.9 and Fig. 5.10 respectively.

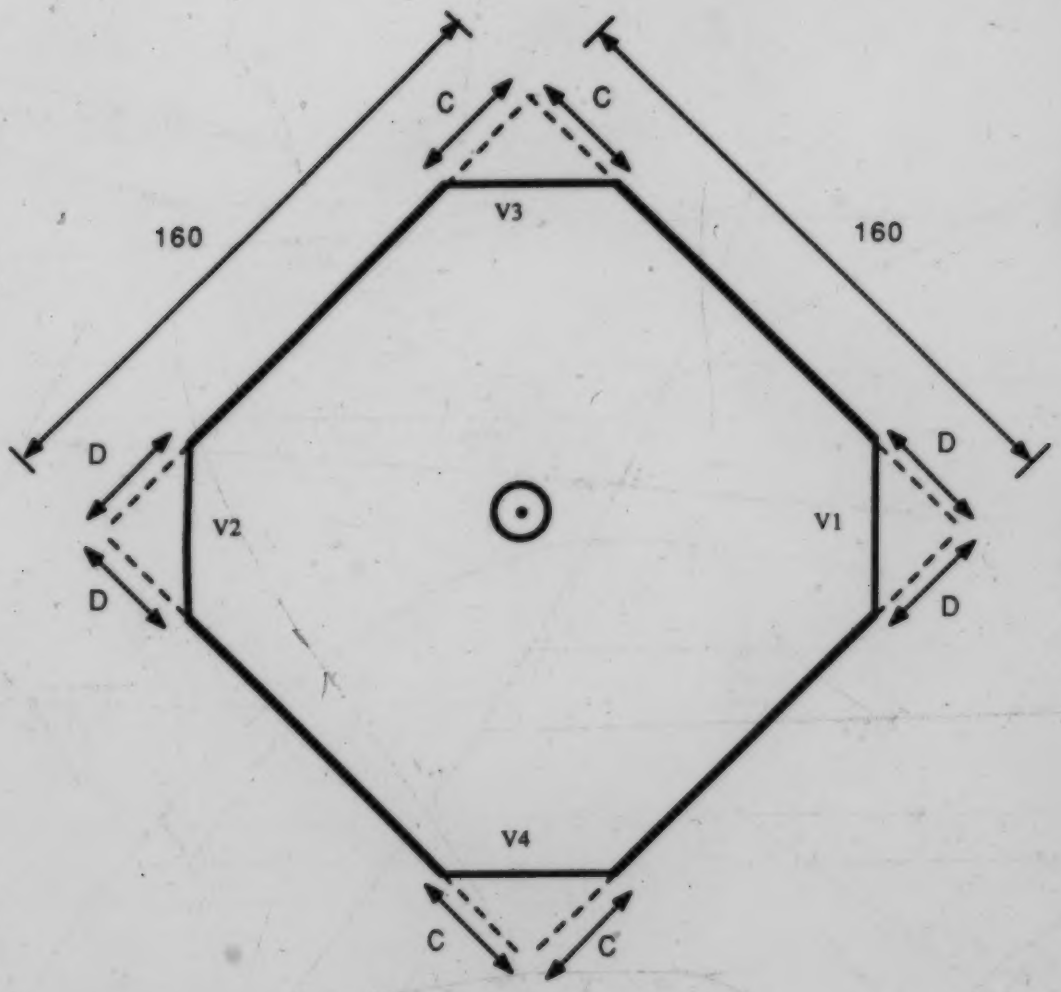


Fig. 5.1 Device domain of Hall plate device

V3 = 5.0 volt  V4 = 0.0 volt
Hall voltage = V1 - V2

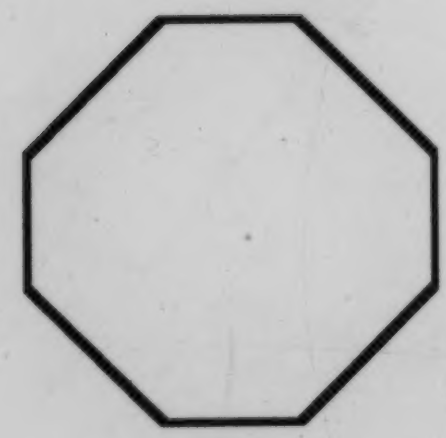

TYPE A

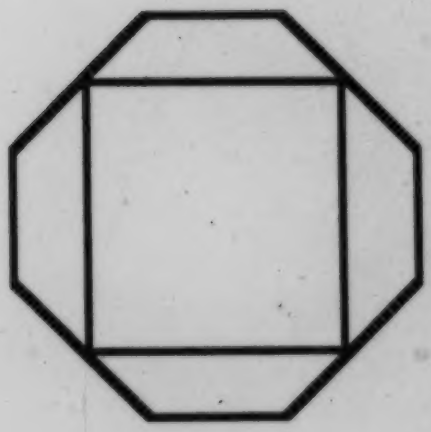

TYPE B

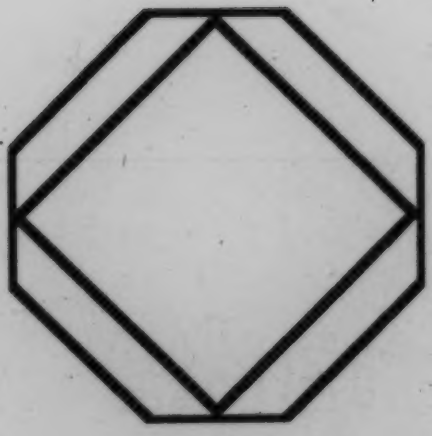

TYPE C

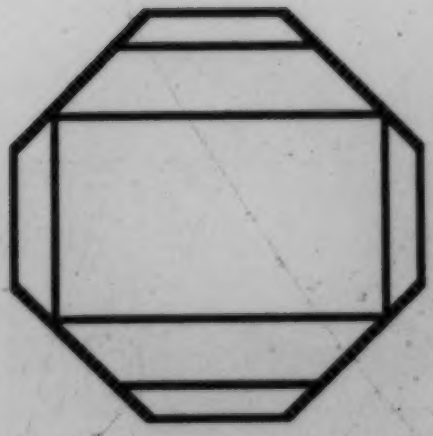

TYPE D

Fig. 5.2 Four types of device geometry setup

Device domain in 3rd quadrant

Device domain after 1st mirroring

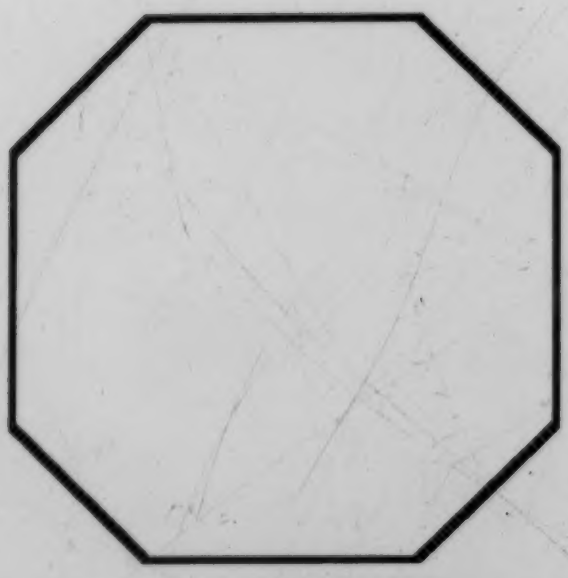

Device domain after second mirroring

Fig. 5.3 Steps involved in generating symmetric mesh

Table 5.1 Hall Voltage Measure

| | C | D | CURRENT(mA) | V1 (V) | V2 (V) | VHALL (mV) | (eff.) L/W |
|---|---|---|---|---|---|---|---|
| 1 | 05 | 05 | 0.33279262 | 2.50092168 | 2.49907831 | 1.84337302 | 3.974e-3 |
| 2 | 10 | 10 | 0.41563603 | 2.50113692 | 2.49886307 | 2.27384475 | 3.182e-3 |
| 3 | 20 | 20 | 0.55624742 | 2.50144870 | 2.49855129 | 2.89740899 | 2.378e-3 |
| 4 | 30 | 30 | 0.69945560 | 2.50167099 | 2.49832900 | 3.34199649 | 1.891e-3 |
| 5 | 40 | 40 | 0.86242804 | 2.50180161 | 2.49819838 | 3.60322694 | 1.533e-3 |
| 6 | 50 | 50 | 1.06588243 | 2.50181703 | 2.49818296 | 3.63407131 | 1.241e-3 |
| 7 | 60 | 60 | 1.35276803 | 2.50168145 | 2.49831854 | 3.36291240 | 9.776e-4 |
| 8 | 70 | 70 | 1.89831284 | 2.50135905 | 2.49864094 | 2.71810793 | 6.967e-4 |
| 9 | 75 | 75 | 2.49881171 | 2.50106825 | 2.49893174 | 2.13650896 | 5.293e-4 |

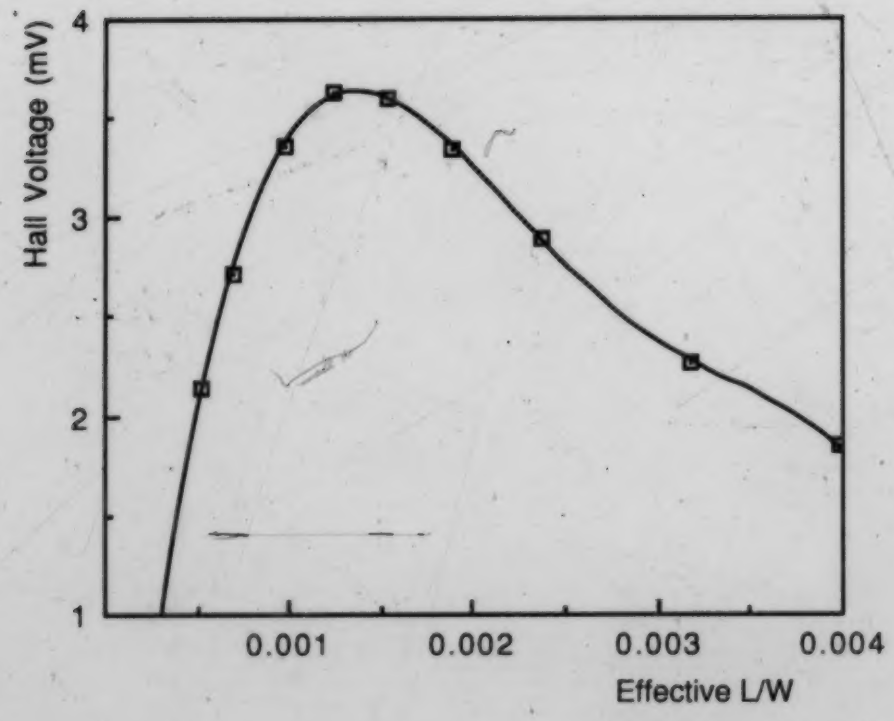


Fig. 5.4 Plot of Hall voltage vs effective L/W

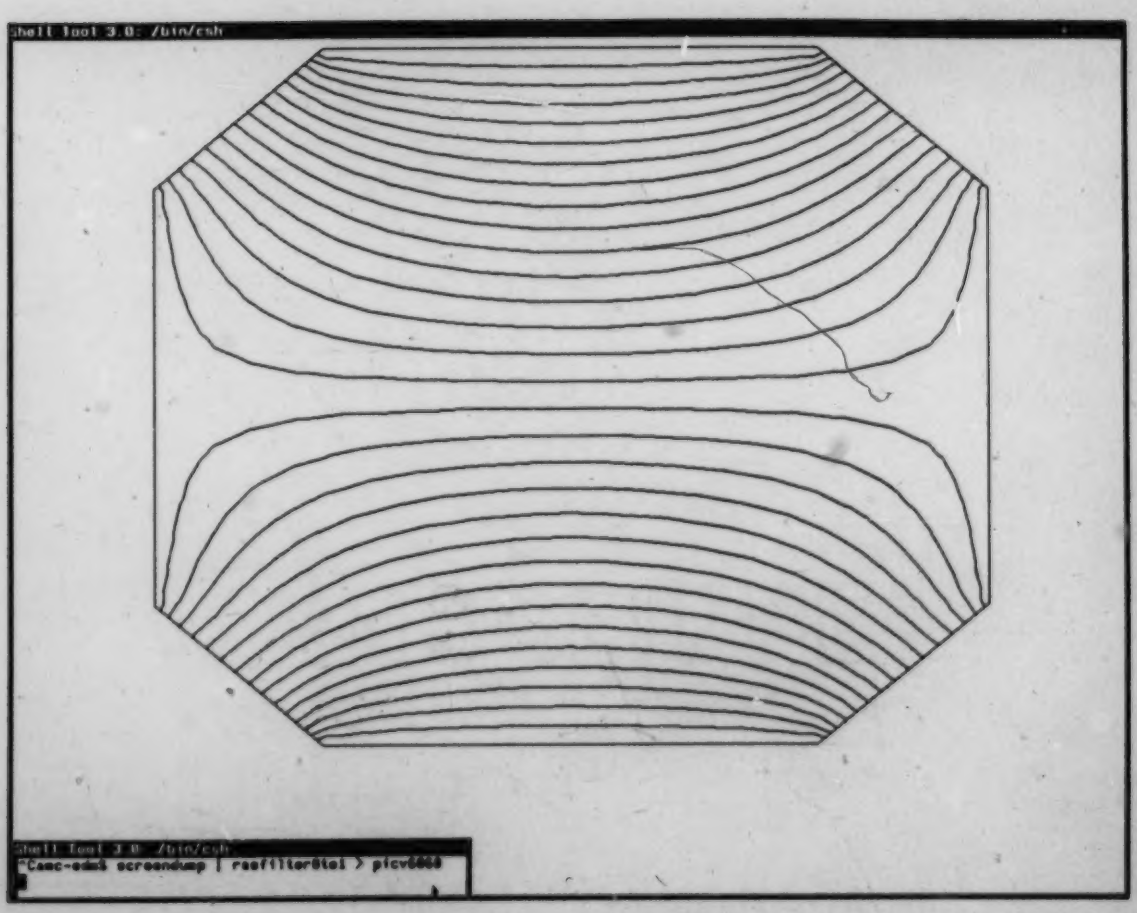


Fig. 5.5 Plot of equipotential lines for Hall plate device

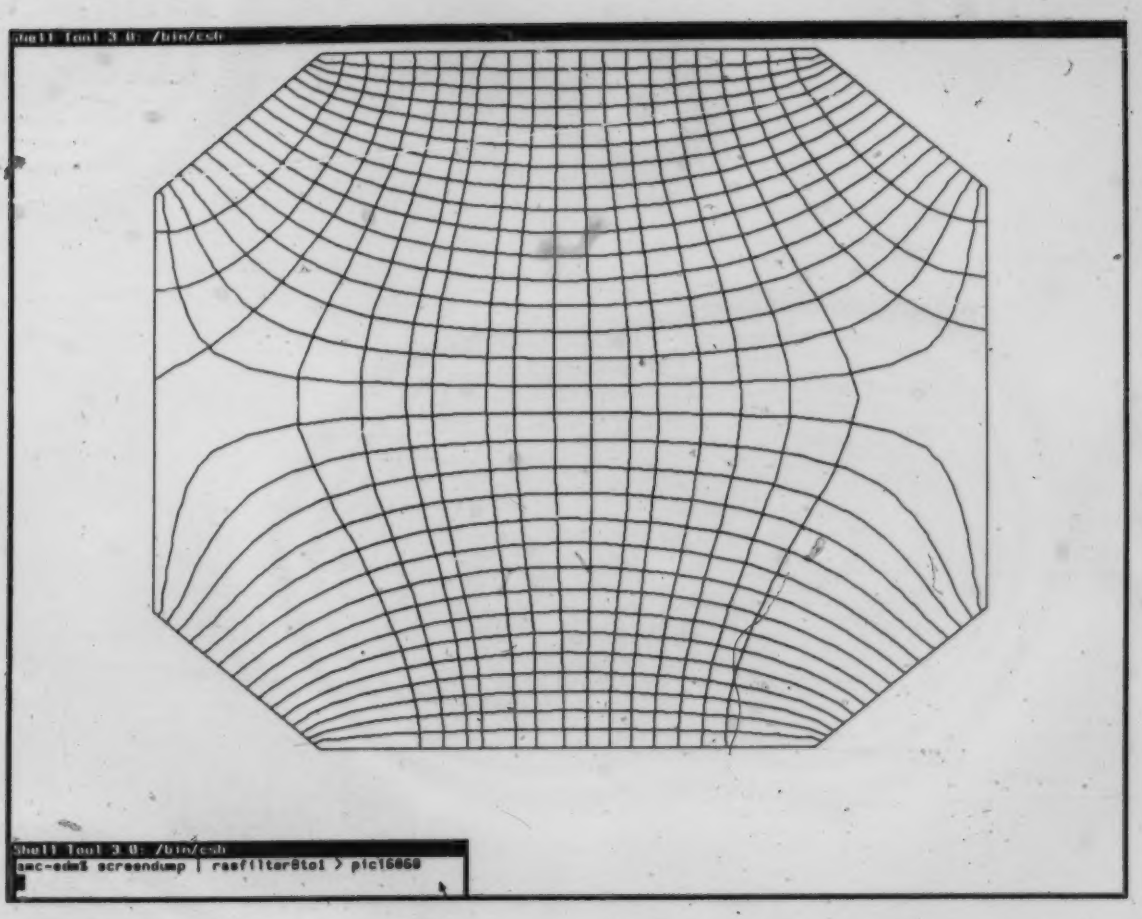


Fig. 5.6 Plot of current density flow for Hall plate device

Table 5.2 Hall Voltage Measure

| | C | D | GEOM. TYPE | CURRENT (mA) | V1 (V) | V2 (V) | VHALL (mV) | (Eff.) L/W |
|---|---|---|---|---|---|---|---|---|
| 1 | 05 | 05 | D | 0.33279262 | 2.50092168 | 2.49907831 | 1.84337302 | 3.974e-3 |
| 2 | 05 | 10 | D | 0.33181038 | 2.50091750 | 2.49908240 | 1.83501828 | 3.986e-3 |
| 3 | 05 | 20 | D | 0.33289100 | 2.50089448 | 2.49910551 | 1.78896729 | 3.973e-3 |
| 4 | 05 | 30 | D | 0.33329271 | 2.50085982 | 2.49914017 | 1.71965437 | 3.968e-3 |
| 5 | 05 | 40 | D | 0.33437762 | 2.50081322 | 2.49918677 | 1.62644213 | 3.955e-3 |
| 6 | 05 | 50 | D | 0.33657325 | 2.50075686 | 2.49924313 | 1.51372075 | 3.929e-3 |
| 7 | 05 | 60 | D | 0.34050333 | 2.50069225 | 2.49930774 | 1.38450257 | 3.884e-3 |
| 8 | 05 | 70 | D | 0.34614415 | 2.50062270 | 2.49937729 | 1.24541753 | 3.821e-3 |
| 9 | 05 | 75 | D | 0.35044495 | 2.50058618 | 2.49941381 | 1.17237629 | 3.774e-3 |
| 10 | 10 | 05 | D | 0.41562649 | 2.50114399 | 2.49885600 | 2.28799695 | 3.182e-3 |
| 11 | 10 | 10 | D | 0.41563603 | 2.50113692 | 2.49886307 | 2.27384475 | 3.182e-3 |
| 12 | 10 | 20 | D | 0.41578247 | 2.50111011 | 2.49888988 | 2.22023858 | 3.181e-3 |
| 13 | 10 | 30 | D | 0.41641695 | 2.50106710 | 2.49893289 | 2.13420572 | 3.176e-3 |
| 14 | 10 | 40 | D | 0.41810215 | 2.50100962 | 2.49899037 | 2.01924724 | 3.163e-3 |
| 15 | 10 | 50 | D | 0.42154134 | 2.50094056 | 2.49905943 | 1.88112151 | 3.137e-3 |
| 16 | 10 | 60 | D | 0.42772577 | 2.50086193 | 2.49913806 | 1.72387536 | 3.092e-3 |
| 17 | 10 | 70 | D | 0.43776914 | 2.50077664 | 2.49922335 | 1.55328757 | 3.021e-3 |
| 18 | 10 | 75 | D | 0.44350951 | 2.50073342 | 2.49926657 | 1.46684369 | 2.982e-3 |
| 19 | 20 | 05 | D | 0.55597131 | 2.50149392 | 2.49850607 | 2.98785140 | 2.379e-3 |
| 20 | 20 | 10 | D | 0.55323833 | 2.50148397 | 2.49851602 | 2.96795566 | 2.391e-3 |
| 21 | 20 | 20 | D | 0.55624742 | 2.50144870 | 2.49855129 | 2.89740899 | 2.378e-3 |
| 22 | 20 | 30 | D | 0.55737010 | 2.50139172 | 2.49860827 | 2.78345849 | 2.373e-3 |
| 23 | 20 | 40 | D | 0.56041459 | 2.50131621 | 2.49868378 | 2.63243238 | 2.360e-3 |
| 24 | 20 | 50 | D | 0.56661746 | 2.50122632 | 2.49877367 | 2.45265910 | 2.334e-3 |
| 25 | 20 | 60 | D | 0.57786084 | 2.50112499 | 2.49887500 | 2.24999124 | 2.289e-3 |
| 26 | 20 | 70 | D | 0.59637316 | 2.50101602 | 2.49898397 | 2.03204730 | 2.218e-3 |
| 27 | 20 | 75 | D | 0.60925783 | 2.50096076 | 2.49903923 | 1.92152777 | 2.171e-3 |
| 28 | 30 | 05 | D | 0.69723989 | 2.50179871 | 2.49820128 | 3.59742281 | 1.897e-3 |
| 29 | 30 | 10 | D | 0.69726662 | 2.50178682 | 2.49821317 | 3.57364019 | 1.897e-3 |
| 30 | 30 | 20 | D | 0.69768164 | 2.50174205 | 2.49825794 | 3.48411905 | 1.896e-3 |
| 31 | 30 | 30 | D | 0.69945560 | 2.50167099 | 2.49832900 | 3.34199649 | 1.891e-3 |
| 32 | 30 | 40 | D | 0.70427284 | 2.50157740 | 2.49842259 | 3.15480813 | 1.878e-3 |
| 33 | 30 | 50 | D | 0.71414285 | 2.50146678 | 2.49853321 | 2.93357384 | 1.852e-3 |
| 34 | 30 | 60 | D | 0.73218664 | 2.50134285 | 2.49865714 | 2.68570152 | 1.806e-3 |
| 35 | 30 | 70 | D | 0.76234807 | 2.50121011 | 2.49878988 | 2.42022751 | 1.735e-3 |
| 36 | 30 | 75 | D | 0.78369182 | 2.50114284 | 2.49885715 | 2.28568921 | 1.688e-3 |
| 37 | 40 | 05 | D | 0.85178119 | 2.50207154 | 2.49792845 | 4.14309288 | 1.553e-3 |
| 38 | 40 | 10 | D | 0.85182140 | 2.50205693 | 2.49794306 | 4.11386929 | 1.553e-3 |
| 39 | 40 | 20 | D | 0.85244771 | 2.50200208 | 2.49799791 | 4.00416169 | 1.551e-3 |
| 40 | 40 | 30 | D | 0.85512394 | 2.50191529 | 2.49808470 | 3.83058922 | 1.547e-3 |
| 41 | 40 | 40 | D | 0.86242804 | 2.50180161 | 2.49819838 | 3.60322694 | 1.533e-3 |
| 42 | 40 | 50 | A | 0.87722375 | 2.50166559 | 2.49833440 | 3.33118207 | 1.508e-3 |

Table 5.2 Hall Voltage Measure

| | C | D | GEOM. TYPE | CURRENT (mA) | V1 (V) | V2 (V) | VHALL (mV) | (Eff.) L/W |
|---|---|---|---|---|---|---|---|---|
| 43 | 40 | 60 | A | 0.90585430 | 2.50151608 | 2.49848391 | 3.03216196 | 1.460e-3 |
| 44 | 40 | 70 | A | 0.95329741 | 2.50135666 | 2.49864333 | 2.71333433 | 1.387e-3 |
| 45 | 40 | 75 | B | 0.98685680 | 2.50127461 | 2.49872538 | 2.54923526 | 1.340e-3 |
| 46 | 50 | 05 | D | 1.02610903 | 2.50230743 | 2.49768256 | 4.61487206 | 1.289e-3 |
| 47 | 50 | 10 | D | 1.02616771 | 2.50228961 | 2.49771038 | 4.57922991 | 1.289e-3 |
| 48 | 50 | 20 | D | 1.02709630 | 2.50222293 | 2.49777706 | 4.44587923 | 1.288e-3 |
| 49 | 50 | 30 | D | 1.03106725 | 2.50211773 | 2.49788226 | 4.23546245 | 1.283e-3 |
| 50 | 50 | 40 | A | 1.04255193 | 2.50197950 | 2.49802049 | 3.95900168 | 1.269e-3 |
| 51 | 50 | 50 | A | 1.06588243 | 2.50181703 | 2.49818296 | 3.63407131 | 1.241e-3 |
| 52 | 50 | 60 | A | 1.10784496 | 2.50163636 | 2.49836363 | 3.27273723 | 1.194e-3 |
| 53 | 50 | 70 | B | 1.18238394 | 2.50144360 | 2.49855639 | 2.88721352 | 1.119e-3 |
| 54 | 50 | 75 | C | 1.23781883 | 2.50134394 | 2.49865605 | 2.68788541 | 1.068e-3 |
| 55 | 60 | 05 | D | 1.23164299 | 2.50250395 | 2.49749604 | 5.00791838 | 1.074e-3 |
| 56 | 60 | 10 | D | 1.21958990 | 2.50246868 | 2.49753131 | 4.93736983 | 1.084e-3 |
| 57 | 60 | 20 | D | 1.23312222 | 2.50240068 | 2.49759931 | 4.80137010 | 1.072e-3 |
| 58 | 60 | 30 | D | 1.23907858 | 2.50227250 | 2.49772749 | 4.54501944 | 1.067e-3 |
| 59 | 60 | 40 | A | 1.25797268 | 2.50210540 | 2.49789459 | 4.21080620 | 1.051e-3 |
| 60 | 60 | 50 | A | 1.29255134 | 2.50190919 | 2.49809080 | 3.81838709 | 1.023e-3 |
| 61 | 60 | 60 | B | 1.35276803 | 2.50168145 | 2.49831854 | 3.36291240 | 9.776e-4 |
| 62 | 60 | 70 | C | 1.47655860 | 2.50145350 | 2.49854649 | 2.90700329 | 8.957e-4 |
| 63 | 60 | 75 | C | 1.57167743 | 2.50132912 | 2.49867087 | 2.65824385 | 8.415e-4 |
| 64 | 70 | 05 | D | 1.48183753 | 2.50265978 | 2.49734021 | 5.31957822 | 8.925e-4 |
| 65 | 70 | 10 | D | 1.47060228 | 2.50261872 | 2.49738127 | 5.23745468 | 8.993e-4 |
| 66 | 70 | 20 | D | 1.48384490 | 2.50252798 | 2.49747201 | 5.05596700 | 8.913e-4 |
| 67 | 70 | 30 | D | 1.49306167 | 2.50237001 | 2.49762998 | 4.74002503 | 8.858e-4 |
| 68 | 70 | 40 | A | 1.52120680 | 2.50216487 | 2.49783512 | 4.32975330 | 8.694e-4 |
| 69 | 70 | 50 | B | 1.57651184 | 2.50192407 | 2.49807592 | 3.84815027 | 8.389e-4 |
| 70 | 70 | 60 | C | 1.68206408 | 2.50165578 | 2.49834421 | 3.31156901 | 7.862e-4 |
| 71 | 70 | 70 | C | 1.89831284 | 2.50135905 | 2.49864094 | 2.71810793 | 6.967e-4 |
| 72 | 70 | 75 | C | 2.08852669 | 2.50119697 | 2.49880302 | 2.39395245 | 6.338e-4 |
| 73 | 75 | 05 | D | 1.61692544 | 2.50270714 | 2.49729285 | 5.41428449 | 8.179e-4 |
| 74 | 75 | 10 | D | 1.62803209 | 2.50268440 | 2.49731559 | 5.36880195 | 8.123e-4 |
| 75 | 75 | 20 | D | 1.61913549 | 2.50256386 | 2.49743613 | 5.12773668 | 8.168e-4 |
| 76 | 75 | 30 | D | 1.64227338 | 2.50239499 | 2.49760500 | 4.78999621 | 8.053e-4 |
| 77 | 75 | 40 | B | 1.67768094 | 2.50216688 | 2.49783311 | 4.33376185 | 7.883e-4 |
| 78 | 75 | 50 | C | 1.74824909 | 2.50189813 | 2.49810186 | 3.79627641 | 7.565e-4 |
| 79 | 75 | 60 | C | 1.89045082 | 2.50159868 | 2.49840131 | 3.19736743 | 6.996e-4 |
| 80 | 75 | 70 | C | 2.19737641 | 2.50126056 | 2.49873943 | 2.52113460 | 6.019e-4 |
| 81 | 75 | 75 | C | 2.49881171 | 2.50106825 | 2.49893174 | 2.13650896 | 5.293e-4 |

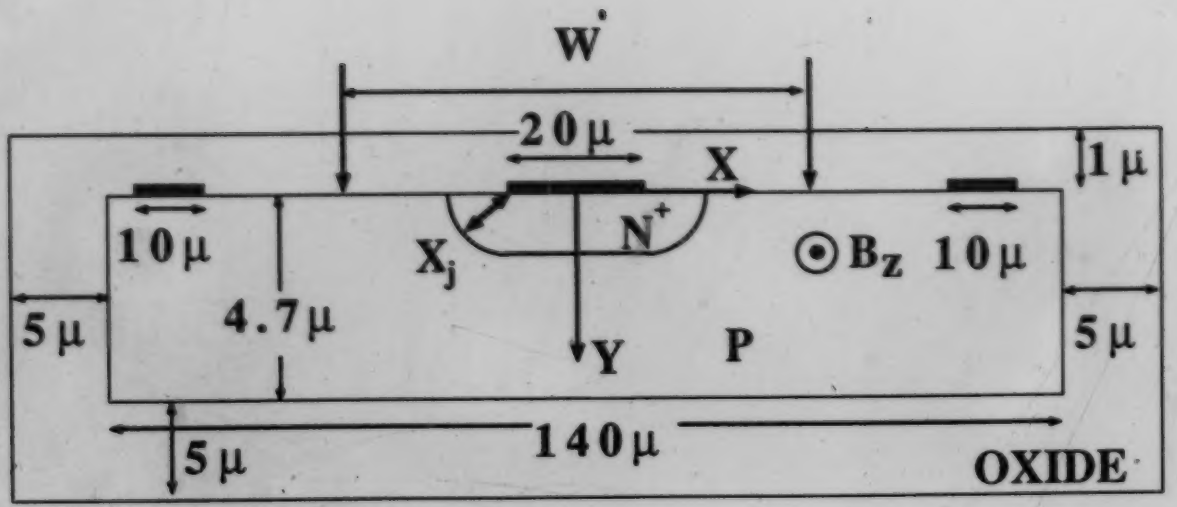


Fig. 5.7 Two dimensional geometry of base region in magnetotransistor

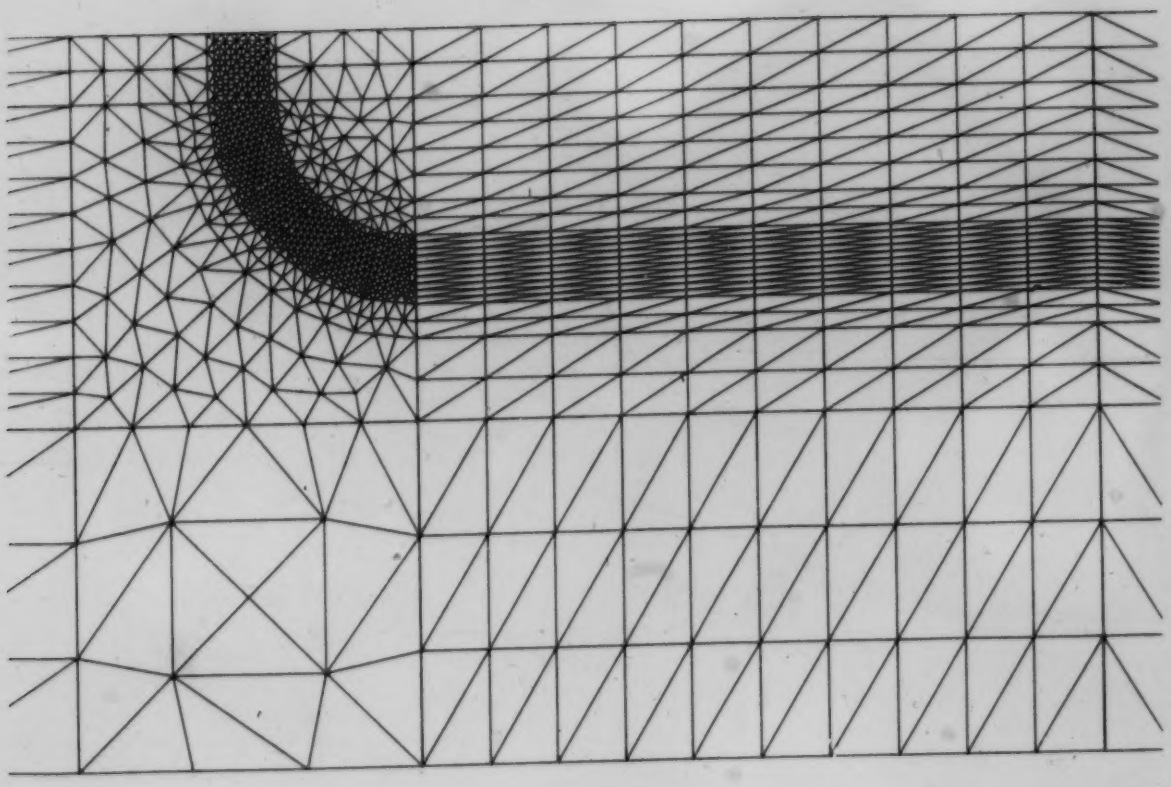

Fig. 5.8 Mesh of emitter-base region in magnetotransistor

Fig. 5.9 Equipotential lines at emitter vicinity for $V_{BE}$=0.85V and B=2T

Fig. 5.10 Minority ( electron) carrier density flow lines at emitter

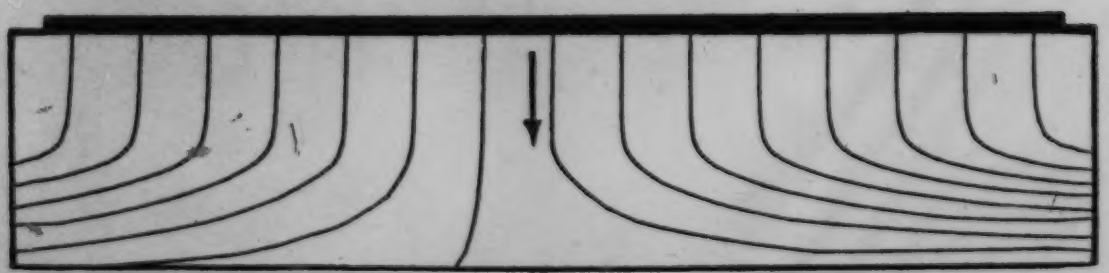

## 6. CONCLUSION AND OUTLOOK

This research was initiated to provide a better design for finite element mesh generation. As a result of this research, we created a new hybrid mesh generator to provide input data for practical finite element semiconductor simulation. It combines the simplicity of a regular triangulation and the flexibility of a Delaunay triangulation. We demonstrated the usefulness of the mesh generator by optimizing a Hall plate device design of commercial value and by simulating a lateral magnetotransistor.

A new hybrid mesh generator has been designed, implemented and incorporated into our magnetic sensor simulation package ALBERTINA to enhance the mesh generation capabilities. This generator can now handle devices of arbitrary polygonal shape and provide interactive mesh modification capabilities to alter part of or the entire device domain to meet the simulation needs. The hybrid approach we used successfully combines and utilizes the advantages of both Delaunay and regular triangulation. It fulfils the five objectives we have identified in Chapter 2. The resulting mesh generator is incorporated so that semiconductor devices with new structures can be simulated.

For the further development of the mesh generation as well as the simulation package, research efforts in the following areas are needed :

1. incorporate more mesh modification functions
2. design parallel algorithm to triangulate individual

concurrently

3. provide error and sensitivity analysis
4. support adaptive mesh generation
5. refine the mathematical model to include mechanical and thermal effects.

The present simulation package deals with magnetic sensors only. In order to simulate a practical semiconductor device more accurately and to investigate other prominent effects inside the device, an improved mathematical model is required. We plan to conduct research to study the thermal and mechanical effects inside a semiconductor device and apply these physical effects to realize better and wider applications.

## REFERENCES


[1] H. P. Baltes and R. S. Popovic, 'Integrated Semiconductor Magnetic Field Sensors', *Proc. IEEE*, vol. 74, pp. 1107-1131, 1986.

[2] S. Selberherr, *Analysis and Simulation of Semiconductor devices*, Springer-Verlag/Wien, pp. 58, 1984.

[3] J. L. Blue and C. L. Wilson, Two-Dimensional Analysis of Semiconductor Devices Using General-Purpose Interactive PDE Sofeware, *IEEE Trans. on Electron. Devices*, vol. ED-30, pp. 1056-1070. 1983.

[4] E. M. Buturla, P. E. Cottrell, B. M. Grossman and K. A. Salsburg, Finite-Element Analysis of Semiconductor Devices: The FIELDAY Program, *IBM J. Res. Develop.*, vol. 25, pp. 218-231, 1981.

[5] G. D. Hachtel, M. H. Mack, R. R. O'Brien and B. Speelpenning, Semiconductor Analysis Using Finite Elements - Part I : Computational Aspects, *IBM J. Res. Develop.*, vol. 25, pp. 232-245, 1981.

[6] W. Fichtner, D. J. Rose, and R. E. Bank, Semiconductor device simulation, *SIAM J. Sci. Stat. Comput.*, vol. 4, pp. 391-415, 1983.

[7] C. L. Wilson and J. L. Blue, Two-Dimensional Analysis of Semiconductor

Devices Using General-Purpose Interactive PDE Sofeware, *IEEE Trans. on Electron. Devices*, vol. ED-30, No. 9, pp. 1056-1070, 1983.

[8] R. Guerrieri, P. Ciampolini, M. Rudan and G. Baccarani, HFIELDS : A Highly Flexible 2-D Semiconductor-Device Analysis Program, *Proc. of NASECODE IV Conf.*, J. J. H. Miller, ed. Dublin: Boole Press, pp. 3-8, 1985.

[9] G. A. Armstrong, R. S. Ferguson and J. Flynn, A Two-Dimensional Finite Element Algorithm for the Simultaneous Solution of the Semiconductor Device Equations with Automatic Convergence, *Int. J. for Num. Meth. in Eng.*, vol 23, pp. 635-644, 1986.

[10] W. Allegretto, Y. S. Mun, A. Nathan and H. P. Baltes, 'Optimization of Semiconductor Magnetic Field Sensors Using Finite Element Analysis', *Proc. of NASECODE IV Conf.*, J. J. H. Miller ed. Dublin: Boole Press, pp. 129-133, 1985.

[11] A. Nathan, 'Numerical Analysis of MOS Magnetic Field Sensors', *M.Sc. Thesis*, The University of Alberta, 1984.

[12] A. Nathan, A. M. J. Huiser, H. P. Baltes, 'Two-Dimensional Numerical Modeling of Magnetic Field Sensors in CMOS Technology', *IEEE Trans. Electron Devices*, vol. ED-28, pp. 1212-1219, 1985.

[13] W. C. Thacker, A brief review of techniques for generating irregular computational grids, *Int. J. for Num. Meth. in Eng.*, vol. 15,

pp. 1335-1341, 1980.

[14] I. Babuska and W.C.Rheinbolt, Mathematical Problems of Computational Decisions in the Finite Element Method, *Proc. of Mathematical Aspects of Finite Element Methods*, Springer-Verlag, pp. 1-26, 1975.

[15] R. B. Simpson, A survey of two dimensional finite element mesh generation, *Proc. 9th Manitoba Conference on Numerical Math. and Computing*, pp. 49-124, 1979.

[16] W. J. Gordon and C. A. Hall, Construction of Curvilinear Coordinate System and Applications to Mesh Generation, *Int. J. for Num. Meth. in Eng.*, vol. 7, pp. 461-477, 1973.

[17] I. Babuska and W. C. Rheinboldt, Error estimates for adaptive finite element computations, *SIAM J. Numer. Anal.*, vol. 15, pp. 736-754, 1978.

[18] J. C. Cavendish, Automatic triangulation of arbitrary planar domains for the finite element method, *Int. J. for Num. meth. in Eng.*, Vol. 8, pp. 679-696, 1974.

[19] A. Bykat, Automatic generation of triangular grid: I - subdivision of general polygon into convex subregions, II - triangulation of convex polygons, *Int. J. for Num. meth. in Eng.*, vol. 10, pp. 1329-1342,

1976.

[20] A. Bykat, Design of a recursive shape controlling mesh generator, Dept. of Mathematics and Computer Science, Emory University, 1982.

[21] M. A. Yerry and M. S. Shephard, A modified quadtree approach to finite element mesh generation, *IEEE Computer Graphics and Applications*, vol. 3, pp. 39-46, 1983.

[22] R. Perucchio, A. R. Ingraffea and J. F. Abel, Interactive Computer Graphic Preprocessing for Three-dimensional Finite Element Analysis, *Int. J. for Num. Meth. in Eng.*, vol 18, pp. 909-926, 1980.

[23] R. B. Simpson, A two-dimensional mesh verification algorithm, *SIAM J. Sci. Stat. Comput.*, vol. 2, pp. 455-473, 1981.

[24] A. Goerge, J. Liu and E. Ng, *User Guide for SPARSPAK*, Waterloo Sparse Linear Equations Package, 1980.

[25] Z. J. Cendes and J. B. Johnson, Application of Delaunay Triangulation to Semiconductor Device Simulation, *Proc. of NASECODE V*, 1986.

[26] Z. J. Cendes, D. Shenton and H. Shahnasser, Magnetic field computation using Delauney triangulation and Complementary Finite Element Method, *IEEE Trans on Magnetics*, vol. Mag-19, pp. 2551-2554,

1983.

[27] M. D. Huang, The Constant-Flow Patch Test - A Unique Guideline for the Evaluation of Discretization Schemes for the Current Continuity Equations, *IEEE Trans on CAD*, vol. CAD-19, pp. 583-608, 1985.

[28] G. Strang and G. J. Fix, *An Analysis of the Finite Element Method*, Pretice Hall, 1973.

[29] Y. S. Mun, 'Numerical Modeling of CMOS Magnetic Field Sensors by Finite Element Method', *M.Sc. Thesis*, The University of Alberta, 1986.

[30] B. Joe, Delaunay Triangulation Meshes in Convex Polygons, *SIAM J. Sci. Stat. Comput.*, vol. 7, pp. 514-539, 1986.

[31] D. T. Lee, Visibility of a simple polygon, *Computer Vision, Graphics, and Image Processing*, vol. 22, pp. 207-221, 1983.

[32] B. Joe and R. B. Simpson, Triangular Meshes for Regions of Complicated Shape, *Int. J. for Num. meth. in Eng.*, vol. 23, pp. 751-778, 1986.

[33] E. M. Buturla, A Finite Element Tutorial, "An Introduction to the Numerical Analysis of Semiconductor Devices and Integrated Circuits", *Short Course of NASECODE II Conf.*, pp. 9-15, 1981.

## APPENDIX A

(mesh examples)

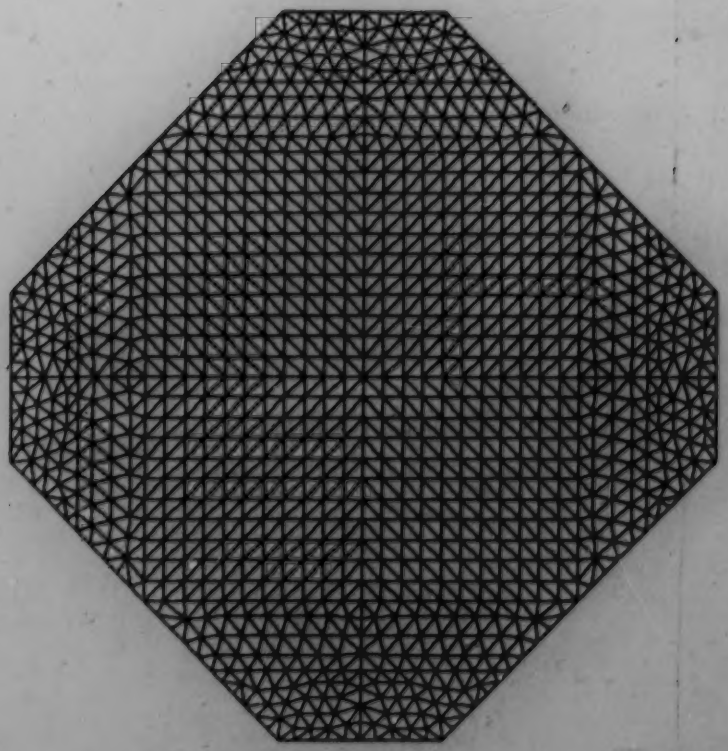

Hybrid triangulation for octagonal region

2040 elements 1089 nodes

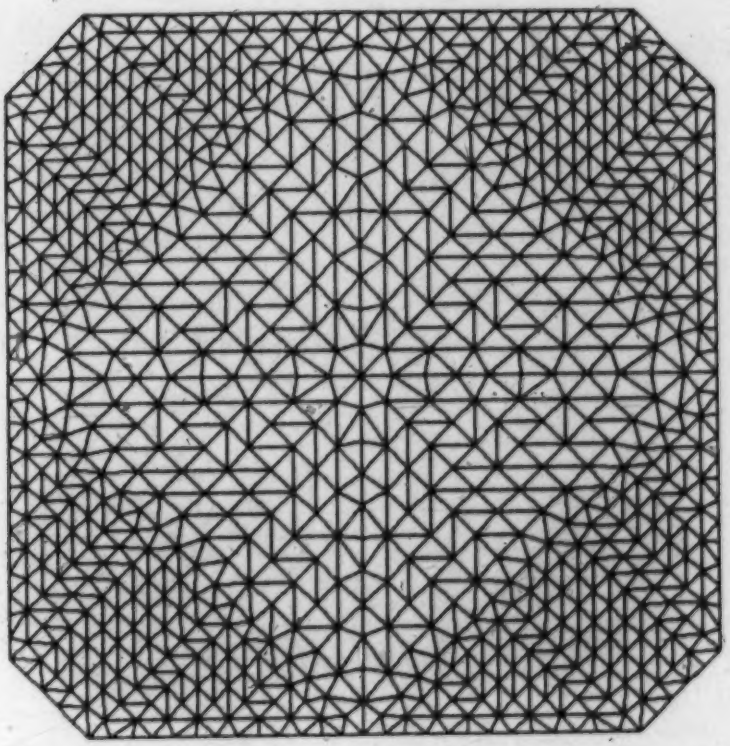

Mesh with type C geometry setup

1572 elements 849 nodes

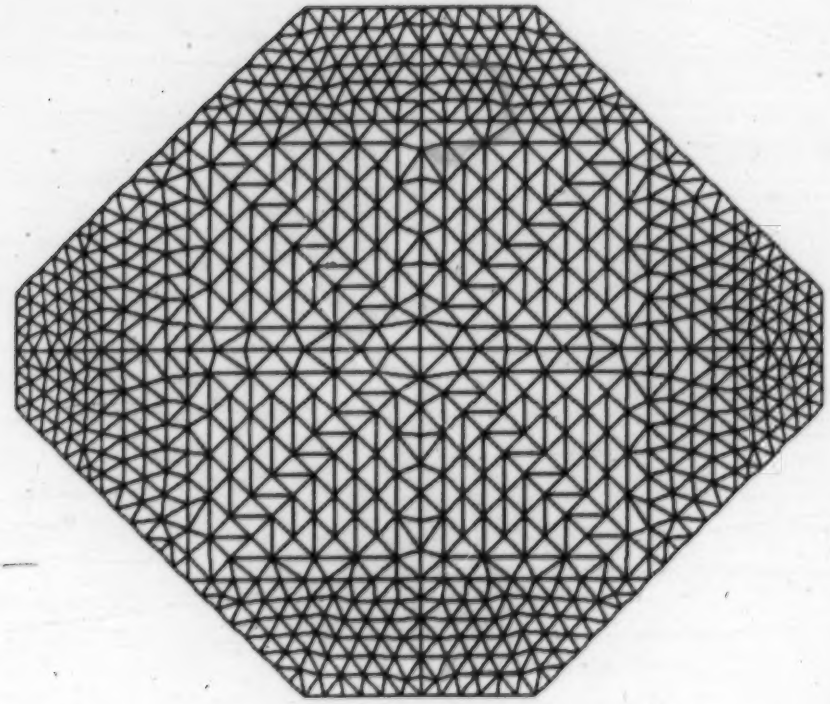

Mesh with type D geometry setup

1420 elements 771 nodes

Delaunay triangulation for a U-shaped region

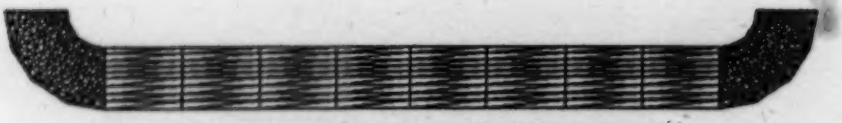

Hybrid triangulation for a U-shaped region

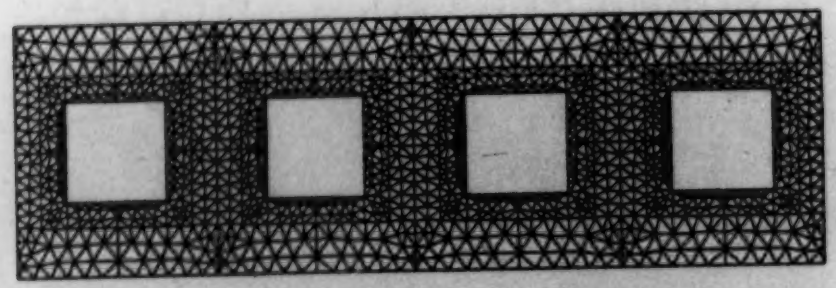

Example mesh for micro-bridge simulation

2192 elements 1241 nodes